NASA/TM—1998-206630

Numerical Modeling of Solidification in Space With MEPHISTO-4 (Part 2)

James E. Simpson
University of Wisconsin, Milwaukee, Wisconsin

Minwu Yao
Ohio Aerospace Institute, Brook Park, Ohio

Henry C. de Groh III
Lewis Research Center, Cleveland, Ohio

Suresh V. Garimella
University of Wisconsin, Milwaukee, Wisconsin

National Aeronautics and
Space Administration

Lewis Research Center

February 1998

This report is a formal draft or working paper, intended to solicit comments and ideas from a technical peer group.

This report contains preliminary findings, subject to revision as analysis proceeds.

Available from

NASA Center for Aerospace Information
800 Elkridge Landing Road
Linthicum Heights, MD 21090-2934
Price Code: A03

National Technical Information Service
5287 Port Royal Road
Springfield, VA 22100
Price Code: A03

Numerical Modeling of Solidification in Space with MEPHISTO-4 (Part 2)

James E. Simpson
University of Wisconsin - Milwaukee
PO Box 784, Milwaukee, WI 53201

Minwu Yao
Ohio Aerospace Institute, Brook Park, OH 44142

Henry C. de Groh III
NASA Lewis Research Center, MS 105-1, Cleveland, OH 44135

Suresh V. Garimella
University of Wisconsin - Milwaukee,
PO Box 784, Milwaukee, WI 53201

ABSTRACT

A pre-flight analysis of the directional solidification of BiSn with MEPHISTO-4 is presented. simplified Bridgman growth under microgravity conditions is simulated using a two dimensional finite element model. This numerical model is a single domain, pseudo-steady state model, and includes the effects of both thermal and solutal convection. The results show that for all orientations of the applied steady state gravity vector, of magnitude 1 μg, the directional solidification process remains diffusion controlled. The maximum convective velocity was found to be 4.424×10^{-5} cm/s for the horizontal Bridgman growth configuration. This value is an order of magnitude lower than the growth velocity. The maximum and minimum values of solute concentration in the liquid at the crystal-melt interface were 13.867 at.% and 13.722 at.%, respectively. This gives a radial segregation value of $\xi = 1.046\%$ at the interface. A secondary objective of this work was to compare the results obtained to those that consider thermal convection only (no solutal convection). It was found that the convective flow patterns in simulations which included solutal convection were significantly different from those which ignored solutal convection. The level of radial segregation predicted by the current simulations is an order of magnitude lower than that found in simulations which ignore solutal convection.

The final aim was to investigate the effect of g-jitter on the crystal growth process. A simulation was performed to calculate the system response to a 1 second, 100 μg gravity impulse acting normal to the direction of growth. This pulse is consistent with that induced by Orbiter thruster firings. The results obtained indicate that such a gravity pulse causes an increase in the level of radial solute segregation at the interface from the steady state values. The maximum value of solute concentration in the liquid was found to be 13.888 at.%, the minimum value calculated was 13.706 at.%, yielding a radial segregation value of ξ = 1.31% at the interface. These values occurred 126 seconds after the pulse terminated. Thus it is anticipated that the process will remain diffusion controlled even when subjected to such g-jitter.

1. INTRODUCTION

The synthesis of advanced materials for the automotive, aerospace, electronic and biomedical fields demands high-quality crystals. The compositional uniformity (and hence the quality) of such crystals can be profoundly influenced by transport phenomena which occur in the melt region. The primary transport mechanism causing these deleterious effects is buoyancy induced natural convection in the melt region. The low gravity environment of space offers an opportunity to suppress the occurrence of buoyancy induced natural convection. Hence there is a great deal of interest in the study of directional solidification of crystals in space.

The MEPHISTO project [1] is a collaborative United States, French and Australian program of space experiments aimed at understanding the fundamental processes involved in crystal growth. The space-borne experimental apparatus is a Bridgman type furnace with an isothermal hot zone, an isothermal chill zone, and an insulated gradient zone. The apparatus was designed and manufactured by the French team. Experiments are conducted on board the Mission-Particular Equipment Support Structure (MPESS) located in the Shuttle's cargo bay. Data acquisition and experiment control is performed remotely from the NASA Marshall Space Flight Center. The MEPHISTO furnace contains three ingots of BiSn (U.S. experiments) or SnBi (French experiments) binary alloy inside fused silica ampoules with a 6 mm inner diameter and a 10 mm outer diameter. All three samples are solidified simultaneously. An identical thermal condition

is imposed on all three samples by two furnaces. A fixed furnace causes the formation of a fixed solid/liquid interface, whilst the moving furnace can facilitate either melting or solidification in the sample. This dual furnace arrangement then causes a region of molten alloy which is bounded by a stationary solid/liquid interface at one end and a moving liquid/solid interface at the other. The apparatus employs the Seebeck technique to determine the moving interface temperature in one sample. The fixed interface is required as a reference for the Seebeck measurements. The moving interface position and shape is determined in the second sample via Peltier pulsing. The final sample is fitted with a resistance measurement circuit which measures the interface velocity, and a rapid quenching capability which enables the solute profile in the liquid near the interface to be captured for post-flight analysis. After flight, the furnace is shipped to France where the samples are extracted. For the U.S. experiments, the samples are returned to the U.S. for post-flight analysis by teams at the University of Florida and the NASA Lewis Research Center.

Three MEPHISTO space experiments have taken place previously, on board United States Microgravity Payload (USMP) -1, -2, and -3 in October 1992, March 1994 and February 1996, respectively. MEPHISTO-4 is scheduled to fly on USMP-4 in November 1997. MEPHISTO-1 and -3 were French experiments which investigated the non-faceted solidification of tin doped with bismuth solute (SnBi). The MEPHISTO-2 and -4 experiments are U.S. experiments that examine the faceted solidification of bismuth doped with a tin solute (BiSn). Alloys based on bismuth are selected for their favorable Peltier and Seebeck coefficients [2].

The principal aims of the MEPHISTO-2 experiments were (i) to examine the interfacial morphological stability threshold of the faceted solid/liquid interface in the absence of convection; (ii) to evaluate the effects of interface kinetics on stability during diffusive, fast diffusive and convective transport regimes; (iii) to examine Bi growth kinetics as a function of supercooling and (iv) to investigate phenomena associated with kinetic roughening [1, 2]. The MEPHISTO-2 experiments used a Bi-0.1 at.% Sn alloy. Two successful melting and solidification cycles were performed. Subsequent to this, experimental anomalies occurred with Peltier pulsing and Seebeck signals. However, fifty-five further melting and solidification cycles

were performed. Finally, 15 cm samples were solidified, with different growth rates, for post-flight microstructural analysis. The loss of reliable Seebeck and Peltier data compromised many of the objectives of the experiment. Despite this, the experimental data resulted in a greater understanding of the dominating role of interface kinetics in morphological stability. Stability phenomena were observed that had not been previously predicted by theory or measured in terrestrial experiments [2].

The MEPHISTO-4 experiment will build on the results of the MEPHISTO-2 experiment and allow information lost due to the anomalies in MEPHISTO-2 to be regained. This experiment will use a Bi-1.0 at.% Sn alloy. Modifications to the experimental apparatus include the addition to each ampoule of a 2mm inner diameter capillary tube, which extends half-way through the process zone. MEPHISTO-2 results indicate that the 6mm cross-section contained a maximum of three grains across the diameter. It is anticipated that the 2mm diameter capillary will facilitate the growth of a single crystal. Thus the Seebeck data for growth inside the capillary can be compared with data obtained for growth beyond the capillary. In this way a comparison of the interfacial kinetics of a single crystal can be compared to the polycrystalline case. Similar orientation-dependent comparisons can be made using the Peltier sample, while the capillary is included in the quenching sample for consistency, and tracking of the resistance change.

2. MEPHISTO: NUMERICAL WORK

The MEPHISTO project includes a program of computational modelling of the crystal growth process. In particular, the role of convection in the melt region is to be investigated by this approach. Accurate experimental determination of convection in metallic melts is very difficult to achieve. The opacity and chemical reactivity of the metallic melts make non-intrusive measurements difficult. Thus numerical investigation of this phenomena is crucial to the complete understanding of the process. Furthermore, the computational models themselves are to be improved by a process involving prediction of, and comparison with, the experimental results. The aim of this procedure is to develop effective fully three dimensional computer simulations of fluid flow related effects [2]. Previously, three-dimensional solutions for

Bridgman growth have been limited to steady state growth in succinonitrile (a widely used transparent phase change material with properties analogous to metallic materials) [3].

One of the critical functions of the supporting computational work is to predict the possible effects of convection in the microgravity environment of space. The microgravity levels which are imposed on the apparatus occur as a result of tidal forces and Shuttle aerodynamic drag. Such accelerations are considered to be quasisteady [4]. The exact orientation of this quasisteady g vector cannot be estimated until late in the flight schedule. The effect of transient g impulses (caused by crew activity or orbital maneuvering - sometimes called "g-jitter") need to be investigated.

During MEPHISTO-1, g-jitter as a result of use of the Orbiter Maneuvering Thrusters (OMS) caused convection in the melt which was observed in the Seebeck measurements. The effects on solute transport of this g-jitter have been modelled by means of a pseudo-steady state model [5]. The results exhibited reasonable agreement with the Seebeck data. A more detailed transient model for MEPHISTO-1 and -2 has been developed, using FIDAP and including front tracking [7]. This model included fully coupled heat transport, solute segregation, fluid motion and phase change. A two-step solution approach was needed to implement front-tracking in addition to solute segregation. Axisymmetric Pseudo-Steady State Models for MEPHISTO-1 and -2 were also developed [7].

There have been other pre-flight computational analyses in support of MEPHISTO-4. For example, sample rehomogenization has been investigated using a variety of finite-difference techniques [8]. This was not a simulation of the solidification process, rather the 2D convection-diffusion equation was solved for the fluid domain in order to determine the time for solute redistribution after a remelting procedure. Both thermal and solutal convection was considered. Results indicated that no additional diffusion time was required for the system to reach an acceptable level of solute uniformity. By means of a transient, 2D FIDAP finite-element model, convection effects at microgravity levels, and in particular the influence of the presence of the growth capillary, for MEPHISTO-4 have also been modelled [9]. The model used a fixed-grid

approach with the enthalpy method being employed to model the phase change. Temporal averaging was used for the apparent heat capacity in the discretized equations. Due to computational difficulties introduced by the small partition coefficient for BiSn, the effects of solute on density, and thus solutally driven convection, were ignored.

A scaling analysis of the convection levels by de Groh and Nelson [4] indicate that solutal convection effects on solute segregation may be significant. However, thus far, it has not been possible to include solutal convection, or even a passive solute into numerical simulations involving phase change for MEPHISTO-4. This is due to the difficulties with convergence with front-tracking methods and difficulties imposed by the low value of partition coefficient for BiSn alloy [7, 9]. The computational modelling presented in this document is intended to examine the effects of thermo-solutal natural convection on the MEPHISTO-4 experiments. A simplified single domain model will be used. These simulations are intended to supplement ongoing work which involves more complex transient, front-tracking models of the process that do not include solutal convection. The simplified model employed is a pseudo-steady state model [5, 6], which considers only the melt region of the solidification process. Effects of solute rejection due to solidification are modeled by an "interface" boundary condition (refer to figure 2) in lieu of including the presence of a solid phase. The key assumptions of the model are that the interface is planar with its temperature dependent on composition, the diffusion-controlled directional solidification is at "steady state," end effects due to the finite length of the ampoule are considered negligible, and the furnace translations rate is equal to the crystal growth velocity. The constitutive equations for mass, heat, species and momentum transport in the fluid region are four coupled, second order, partial differential equations. Solutions to these equations will be obtained using the commercial finite element CFD package FIDAP.

Simulations will be performed for cases involving a steady g vector (representing tidal and drag forces) of constant magnitude. The direction at which the g vector acts will be varied for each case. In addition, a transient simulation will be performed to investigate the system response to g-jitter. A g-pulse will be used which is consistent with that imposed by the thrusters of the shuttle during standard orbital maneuvering.

3. MATHEMATICAL FORMULATION

3.1 Governing Equations

For this work, we shall consider the melt region during the directional crystal growth of a binary alloy by the Bridgman process (refer to figure 1). The melt is considered to be a viscous, heat-conducting Newtonian fluid subject to thermo-solutal convection. Thermophysical properties are dependent on temperature while density variations in the fluid are considered subject to the Boussinesq approximation.

The principle of conservation of momentum is then governed by the Navier-Stokes equation

$$\rho_0\left(\frac{\partial \mathbf{u}}{\partial t}+\mathbf{u}\cdot\nabla\mathbf{u}\right) = \rho_0\mathbf{g}\left[1-\beta_T(T-T_0)-\beta_C(C-C_0)\right]-\nabla P+\nabla\cdot\left[\mu\left(\nabla\mathbf{u}+(\nabla\mathbf{u})^T\right)\right] \tag{1}$$

where $\mathbf{u}$ is the velocity vector, ρ_0 is the fluid density at the reference temperature T_0 and initial solute concentration C_0, T is temperature, $\mathbf{g}$ is the gravitational acceleration vector, β_T and β_C the volumetric expansion coefficients due to temperature and solute[1] concentration, μ is the first coefficient of viscosity and P is the pressure. Since density variations are limited to the buoyancy term in equation (1), the governing equation for the principle of conservation of mass reduces to the divergence free condition

$$\nabla\cdot\mathbf{u} = 0 \tag{2}$$

The equation for the transport of energy is a second order partial differential equation

---

[1] The units of β_C, and $(C - C_o)$ in $\beta_C(C-C_o)$ of (1) were $(\text{atomic fraction})^{-1}$ and atomic fraction respectively; this was an error resulting in a larger $\beta_C(C-C_o)$ product. The proper units of β_C and C are $(\text{volume fraction})^{-1}$ and volume fraction. See Postscript notes, section 7, for a discussion.

$$\rho_0 c_p \left(\frac{\partial T}{\partial t} + \mathbf{u} \cdot \nabla T \right) = \nabla \cdot (\kappa \nabla T) \tag{3}$$

in which κ is the thermal conductivity and c_p is the specific heat capacity. The governing equation for the conservation of solute concentration is

$$\frac{\partial C}{\partial t} + \mathbf{u} \cdot \nabla C = \nabla \cdot (D \nabla C) \tag{4}$$

where C is the atomic fraction of solute and D is the diffusion coefficient of the solute (Sn) in the solvent (Bi).

The model under consideration is a pseudo-steady state model similar to that by Alexander *et. al.* [6]. This is a single domain model which only considers the melt region of the solidification process. Thus constitutive equations (1) to (4) are continuous over the entire simulation domain and no solid-liquid interface matching conditions need to be developed. However, the temperature of the pseudo interface is allowed to change due to changes in solute concentration in compliance with the equilibrium phase diagram.

Now that the constitutive equations have been introduced, initial conditions and boundary conditions need to be specified so that the problem becomes fully defined and a solution may be sought.

3.2 Initial and Boundary Conditions

The pseudo-steady state model (PSSM) is a widely used model for the simulation of steady-state Bridgman crystal growth. There are many variants of this model, the simplest being single-domain solutions that consider the solid/liquid interface to be flat with a constant melting temperature [5, 6]. More complex variants may include the presence of a solid [7]. For the present work, we will improve the single-domain steady state model of Alexander [5] and

Alexander *et. al.* [6] by including the effects of a concentration dependent solid/liquid interface temperature and solutal convection. This new idealized model is shown in figure 2. The assumptions that underpin this new model are 1) that the interface is considered to be planar and its temperature concentration dependent, 2) the diffusion controlled directional solidification is at "steady state," making the *average* composition at the s/l interface C_o, 3) end effects due to the finite length of the ampoule are negligible, 4) the furnace translation rate is equal to the crystal growth velocity,[2] and 5) the (steady state) concentration profile used is a reasonable approximation of the profile expected during the (transient) process. Translation of the ampoule relative to the furnace is modelled by translating the coordinate axes at a rate equal to the growth velocity. This results in a continuous slug of melt moving opposite to growth velocity ($-u_g$) and at the bulk solute composition C_0 being supplied through the inlet. The "inlet" or "far field" boundary conditions then are (from ref. [5, 6])

$$\text{at } x = x_f: \qquad u_x = -u_g, \qquad u_y = 0, \qquad T = T_h, \qquad \frac{\partial C}{\partial x} = -\frac{u_g}{D}\left(C - C_0\right) \tag{5}$$

in which T_h is the hot zone temperature. The effect of solute-poor material solidifying at the crystal-melt interface is modelled by the boundary conditions applied at the "interface" boundary. Since we have assumed that the crystal growth rate is equal to the furnace translation rate, the interface boundary is located at a fixed distance L from the inlet. Since the freezing temperature of a binary alloy is dependent on the solute concentration (refer to figure 4), the interface temperature will be considered variable with concentration. Thus, the boundary conditions applied at the interface boundary become (from ref. [5, 6])

$$\text{at } x = x_i: \qquad u_x = -u_g, \qquad u_y = 0, \qquad T = T_m + mC, \qquad \frac{\partial C}{\partial x} = -\frac{u_g}{D}(1-k)C \tag{6}$$

---

[2]Because of the solute build up at the interface, this may not be true during the initial transient. However, because of the large temperature gradients, the interface quickly catches up with the furnace translation.

in which T_m is the melting temperature of pure bismuth, m is the slope of the liquidus line (refer to figure 4) and k is the partition (or segregation) coefficient for a BiSn alloy. The ampoule walls are considered to be impermeable to solute and translate at the growth velocity,

$$\text{at } y = \pm R: \qquad u_x = -u_g, \qquad u_y = 0, \qquad \frac{\partial C}{\partial y} = 0 \tag{7}$$

in which R is the ampoule inner radius (half simulation domain height). For the thermal boundary conditions, there is an initial adiabatic length near the interface and the remainder of the walls are at the furnace temperature

$$\text{at } y = \pm R: \qquad \frac{\partial T}{\partial y} = 0 \quad \text{for } x_i \le x < x_a, \qquad T = T_h \quad \text{for } x_a \le x \le x_l \tag{8}$$

in which x_i, x_a and x_l are the interface, end of adiabatic zone and inlet x locations, respectively.

The initial conditions employed for the steady state solutions were

$$u_x = -u_g, \qquad u_y = 0, \qquad T = T_h \qquad C = C_0 \tag{9}$$

3.3 Concentration Modification

Boundary conditions for concentration (5) and (6) implicitly assume that, for concentration, a one dimensional "steady-state" growth mode exists. During steady state growth, the concentration of the solid at the interface is equal to the far-field value of concentration (C_0 = 1 at.%). The concentration in the liquid is given by the equation (from ref. [10, 11])

$$C_L = C_0\left[1 + \frac{1-k}{k}\exp\left(-u_g x'/D\right)\right] \tag{10}$$

in which x′ is the distance from the front into the melt. Note that this analytical solution has been obtained by assuming a constant value for diffusion coefficient, D. Due to the low value of partition coefficient, k, for the BiSn alloy system considered in this work, the diffusion-controlled growth is in the "initial transient" regime throughout the entire experiment. Thus the steady state concentration profile in the liquid is never encountered in the experiment. The concentration values calculated by the steady state model were found to be unrealistic; in particular it predicted concentration values which would lead to the formation of the second phase (Sn-rich) at the interface. The model was altered so that it would furnish a more realistic concentration profile. The most effective way to achieve this end was to retain boundary conditions (5) and (6), and simply alter the far-field concentration value, C_0, and thus the average solid composition at the interface, changing them to C_s^*. The value of C_s^* was determined using the equation for the concentration at the solid interface, during the initial transient, with diffusion controlled growth (from ref. [10, 11])

$$C_s^* = C_0\left[1 - (1-k)\exp\left(-k u_g z/D\right)\right] \qquad \text{(for } k \le 0.1\text{)} \tag{11}$$

In which z is the distance over which solidification has occurred. The result after growth has progressed for 1.5 cm is $C_s^* \approx 0.4$ at.%. The value of C_0 selected was then 0.4 at.%. Figure 5 is a plot of the steady state profile yielded with this new value. A constant diffusion coefficient of $D = 3.0 \times 10^{-5}$ cm^2/s (which is the value for D at 550 K, refer to table A1) was used. This altered model then constitutes the *concentration modified pseudo steady state model (CM-PSSM)*. Its utility is that it enables us to investigate the effects of thermo-solutal convection on the solidification process. This compromise was necessary since more realistic models, involving a full transient analysis with front-tracking, have not been able to include the effects of solute [9], yet it is strongly desired to gauge the effect of solutal gradients on convection, since those effects are expected to be of the same order of magnitude as those thermal driven [4,8].

In summary, a new steady-state model known at the concentration modified pseudo steady state model (CM-PSSM) has been proposed. The key assumptions employed in formulating this model are 1) the interface is planar and its temperature is concentration dependent, 2) a "steady state" mode of directional solidification exists, 3) end effects are negligible, 4) the furnace translation rate is equal to the growth velocity, and 5) the (steady state) concentration profile used is a reasonable approximation of the profile expected during the (transient) process. Note that no constitutional supercooling in the melt is incorporated in the model.

Now that the constitutive equations, initial conditions and boundary conditions have been specified for the model, an appropriate numerical solution scheme needs to be determined so that a solution may be obtained to the problem posed.

4. NUMERICAL ANALYSIS

4.1 Discretization and Solution Scheme

Numerical solutions are obtained via the commercial finite element CFD code FIDAP (release 7.6). Four node quadrilateral finite elements were used. Bilinear shape functions for velocity, temperature and concentration were employed. Linear interpolation for pressure (discontinuous at the element boundaries) was used. Further details of this finite-element formulation may be found in [12]. The FEM discretization of equations (1) to (4) results in a set of strongly-coupled nonlinear algebraic equations. For the steady g simulations (presented in section 5.1), a Picard iteration scheme was used to solve these equations. This involved applying a single iteration of successive substitution (large radius of convergence, slowly convergent) followed by nonlinear Newton-Raphson iterations (small radius of convergence, quickly convergent). Convergence of the iterative scheme is assessed using the following criteria

$$\frac{\|\mathbf{u}^{p} - \mathbf{u}^{p-1}\|}{\|\mathbf{u}^{p-1}\|} \leq 10^{-3} \tag{12}$$

$$\frac{\|\mathbf{R}^p\|}{\|\mathbf{R}^0\|} \leq 10^{-3} \tag{13}$$

in which **u** represents the solution vector (of the field variables velocity, temperature and concentration), **R** is the residual vector, p denotes the iteration number and the L_2 *norm* is defined as (from ref. [13])

$$\|\mathbf{x}\| = \left(\Sigma_j^n |\mathbf{x}_j|^2 \right)^{1/2} \tag{14}$$

where n is the length of the vector and j is a dummy index. The tolerance value used (10^{-3}) is an order of magnitude smaller than the FIDAP default value and has been used in previous work [3]. Convergence occurred after no more than 5 iterations for all cases studied. Computations were carried out on a Silicon Graphics Power Challenge workstation with four 90 MHz processors. The CPU burden was typically 50-58 seconds. For the transient simulations involving a g impulse (presented in section 5.2), solution at each time step was achieved via a Newton-Raphson iteration scheme. The same convergence criteria were employed. Fully implicit time integration was used with a variable time step. The minimum and maximum time steps used were 0.05 and 8 seconds, respectively. Computations were performed on the same platform as for the steady g simulations. A total of 505 time steps were calculated, for a final finish time of 1,140 seconds. The CPU requirement was 5,600 seconds.

4.2 Grid Independence Study

The mesh used is shown in figure 3. There are a total of 60 finite elements in the x-direction and 18 finite elements in the y-direction. Half of the total number of finite elements are located within the adiabatic zone, with the elements being progressively graded as the crystal-melt interface is approached. This is to ensure an efficient placement of elements near the crystal-melt interface where solutal gradients are large. To determine the adequacy of this discretization, simulations were performed using three different mesh sizes, for a test case with a constant gravity vector of 1 μg oriented at $\theta = 0^{\circ}$ (horizontal Bridgman growth). The flow-field results indicated that the 60 × 18 discretization was appropriate, since the variables examined did not change by more than 1% at the next highest level of mesh refinement. The results of this study are summarized in Table 1. The field variables examined were

- $|U_{max}|$, the maximum value of velocity throughout the flow domain. The value of growth velocity is subtracted from the velocity vectors used to determine this calculation (refer to section 5.1). The location of this quantity is also given.
- T_{mid}, the value of temperature in the midpoint of the adiabatic zone (x = 4.77305 cm, y = 0 cm). This quantity has been used in the literature to test convergence for natural convection in a closed cavity [14, 15].
- C_{mid}, the value of concentration at the interface boundary and on the centerline. This location was selected in the absence of a "natural" test location. It should be noted that the concentration profiles were almost identical for all three meshes (indicating that the mesh grading is effective in resolving the diffusion-controlled solute boundary layer).

The CPU burden required is also given in the table. Note the difficulties encountered in achieving convergence at the coarsest mesh.

Table 1. Summary of grid independence results (quantities in brackets indicate the percent change between the value found using the present mesh and at the next most refined mesh).

Mesh	$\|U_{max}\| \times 10^5$ (cm/sec)	$\|U_{max}\|$ location (x cm, y cm)	T_{mid} (K)	C_{mid} (at. %)	CPU (sec/# iterations)
30 × 9	4.514 (2.03%)	(5.123, 0.1667)	755.0 (0.453%)	13.7921 (0.001%)	101/29
60 × 18	4.424 **(0.6827%)**	(5.132, 0.1667)	751.6 **(0.173%)**	13.7919 **(0.001%)**	58/5
120 × 36	4.394	(5.137, 0.1667)	750.3	13.7918	468/5

5. RESULTS

5.1. Steady Gravity Vector

Simulations were performed for a **g** vector of constant magnitude 1 μg at a variety of orientations (the definition of angle θ is provided in figure 2). The orientations considered were θ = 0° (horizontal Bridgman growth), +22.5°, +45°, +67.5°, +90° (vertical Bridgman growth, crystal at top) -45° and -90° (vertical Bridgman growth, crystal at bottom) degrees. The most pertinent results were for the θ = 0°, +45°, +90° and -90° configurations because residual gravity in MEPHISTO-4 is expected to be 1μg at +45° and previous MEPHISTO modeling has considered gravity vectors acting at 0° and -90°. These will be presented in depth in this section while plots of the results for the remaining configurations are provided in appendix A. In addition, supplementary simulations were performed which excluded the effect of solutal convection and considered thermal convection only. The orientations considered were θ = 0°, +45°, +90° and -90° degrees. The purpose of these supplementary calculations is to provide a comparison with results obtained in the cases which included solutal convection, and hence aid in the determination of the importance of solutal convection on the interface solute concentration levels.

Thermophysical properties and other constants used in obtaining the solution are provided in table A1 in the appendix. Note that the x locations of the interface, end of adiabatic zone and inlet were taken to be x_i = 3.94805 cm, x_a = 5.59805 and x_l = 11.25 cm. These values were consistent with the simulations for MEPHISTO-4 in ref. [9].

Figure 6 (a) is a plot of velocity vectors for the case of $\theta = 0^\circ$ (horizontal Bridgman growth). Note that the growth velocity component has been subtracted from these plots for clarity. Also note that the entire domain is not shown; the x range of the plots is smaller than the cavity length in order to highlight details near the interface. The main feature of the results is that there are two counter-rotating convective cells in the flow domain. The primary convective cell, which is driven by thermal gradients, rotates in a counter-clockwise fashion. The length of this convective cell is approximately 2.1 cm resulting in aspect ratio (height:length) of 0.29. The maximum velocity in the domain occurs in this thermal convective cell. The magnitude of the maximum velocity is 4.424×10^{-5} cm/s (an order of magnitude lower than the growth velocity) at a location of (5.132, 0.1667) cm. As will be shown later, at these velocities diffusive transport is dominant over convective transport. The secondary convective cell, driven by solutal gradients, is near the interface. This cell is 0.172 cm long with an aspect ratio (height:length) of 3.49. The velocities in this cell are smaller than in the primary cell. In particular, the velocities are very small near the interface, for example, the velocity at (x = 3.9462 cm, y = 0 cm) is only 3.873×10^{-6} cm/s. Figure 6 (b) is a plot of the density variation in the buoyancy term of equation (1). This plot makes the net driving force behind the convective motion seen in figure 6 (a) readily apparent. At the interface, solute rejection leads to high levels of solute. This opposes the tendency of the fluid density to increase in response to the low temperatures near the interface. The net result is that the fluid is *below the reference density* at the interface (note that Sn is lighter than Bi). Moving away from the interface, the solute concentration decays while temperatures steadily increase. The net result is a region of maximum density located between the two convective cells seen in figure 6 (a). Further away from the interface, the density decreases linearly in the adiabatic zone. Near the end of the adiabatic zone the density contours exhibit curvature. Past the adiabatic zone the density takes on a minimum

value. Figure 7 (a) is a plot of solute concentration contours for this gravity orientation. Note the finer scale used on the x-axis (x range to 6 cm). The main feature to note is that the solute concentration lines remain flat. This indicates that convective effects on the solute boundary layer are negligible and so the growth is dominated by diffusion. Figure 7 (b) is a plot of the temperature contours for the same case. Again, convection has not significantly distorted the isotherms. Note also the curvature of the isotherms at the end of the adiabatic zone (x = 5.59805 cm). These are due to heat being conducted in from the hot zone. The minimum temperature at the interface is 512 K; this is lower than the reference value of 544.3 K since the solute concentration at the interface has suppressed the melting temperature. The interplay of concentration levels indicated in figure 7 (a) and the temperatures shown in figure 7 (b) result in the density contours shown in figure 6 (b).

Figure 8 (a) is a plot of velocity vectors for a gravity orientation of θ = +45°, i.e. equal components of gravity acting in the negative y direction and horizontally away from the interface in the positive x direction. As for the horizontal growth case detailed above, the most important feature is the presence of two counter-rotating convective cells. The character and dimensions of the cells are identical to those in the horizontal case, however the velocities are smaller in magnitude. The maximum velocity occurs in the primary convective cell. Its magnitude is 3.132 $\times$ 10^{-5} cm/s at a location of (x = 5.132 cm, y = 0.1667 cm). The ratio of the maximum velocities for this orientation to that found for horizontal Bridgman growth is 0.707. This is also the ratio of the y gravity components, highlighting the direct relationship between y gravity component and the resulting level of convection. There is no discernible difference between the plots of density, solute concentration and temperature contours for this case and those provided in figures 6 (b), 7 (a) and 7 (b) and so they have been omitted. Figure 8 (b) is a plot of velocity vectors for a gravity orientation of θ = +90°, i.e. anti-vertical Bridgman growth with the gravity vector pointing away from the crystal and into the melt. For this orientation, concentration gradients are stable while temperature gradients are unstable. As there is no longer a y gravity component, the character of the convective motion has changed compared to the convective motions exhibited in the previous two cases. For the θ = +90° configuration, two convective cells exist in the region at the end of the adiabatic zone. The cells are mirror images of each other about the x-

axis. The velocities at the x-axis (y = 0) are in the positive x direction. The maximum velocity is 3.0498 $\times 10^{-6}$ cm/s at a location of (x = 5.718 cm, y = 0 cm). This is two orders of magnitude lower than the value of growth velocity, and approximately 12 times slower than the maximum velocity for the $\theta = 0^{\circ}$ case. Because of the low gravity magnitude no Rayleigh-Bénard style convective instabilities [16] are observed. Since there are no thermal or solutal gradients normal to the direction of the gravity vector, convection is absent near the interface. Thus conditions at the interface are completely diffusion controlled. Again, there is no discernible difference between the plots of density, solute concentration and temperature contours for this case and those for $\theta = 0^{\circ}$ so they have been omitted. Figure 8 (c) is a plot of velocity vectors for a gravity orientation of $\theta = -90^{\circ}$, i.e. vertical Bridgman growth with the gravity vector pointing down at the crystal. For this orientation, concentration gradients are unstable while temperature gradients are stable. The important detail to note is that the convective motions operate in the reverse sense to those for the $\theta = +90^{\circ}$ case, such that the flow at the centerline is in the negative x direction.

The next step in our analysis is to assess the impact of these solutal-convective motions on the solute segregation at the interface (and hence the solute segregation in the solid). Figure 9 shows solute concentration values across the interface ($x = x_i = 3.94805$ cm), for each gravity angle θ tested. For the anti-vertical and vertical Bridgman growth configurations ($\theta = \pm 90^{\circ}$), concentration remains constant since conditions at the interface are completely diffusion controlled. For other values of θ, the presence of convective transport causes concentration to vary slightly across the interface. The minimum and maximum values of concentration occur at y = -0.3 cm and y = +0.3 cm, respectively. As θ moves from $+90^{\circ}$ to 0°, the difference between maximum and minimum concentrations increases. The maximum disparity between minimum and maximum concentrations occurs for the $\theta = 0^{\circ}$ case, corresponding to the maximum level of convection. For this orientation, C_{max} = 13.867 at.%, C_{min} = 13.722 at.%. These values correspond to 0.402 at.% and 0.398 at.% in the solid.

Figure 10 is a plot of radial solute segregation, ξ, against gravity angle, θ. The radial solute segregation is defined as

$$\xi = \frac{100\% \times \left(C_{max} - C_{min}\right)}{C_{av}} \tag{15}$$

C_{av} is taken to be the average value across the interface (a lateral average [7]). The maximum value of segregation is 1.046% for $\theta = 0^{\circ}$. The authors consider this value of segregation to be negligible. This confirms that the levels of convection are small, the process is diffusion-dominated. As angle θ increases, the segregation level decreases. Note that the level of segregation decreases much more rapidly with θ as $\theta \rightarrow +90^{\circ}$. At $\theta = +90^{\circ}$, the pure diffusion orientation, there is zero segregation.

What remains now is to compare and contrast these results to a case in which solutal convection is ignored. Figure 11 (a) is a plot of velocity vectors for a simulation with $\theta = 0^{\circ}$ and thermal convection only. In contrast to the results for thermo-solutal convection, there is a single, dominant counter-clockwise rotating convective cell. The length of this convective cell is about 2.25 cm with an aspect ratio (height:length) of 0.266. The maximum velocity is 4.427×10^{-5} cm/s (slightly larger than the thermo-solutal case) acting at a location of (x = 5.1324 cm, y = 0.1667 cm). which is identical to that found in the thermo-solutal case. The maximum velocities *within the solutal boundary layer* are 5.450×10^{-6} cm/s and 1.969×10^{-5} cm/s for the cases including and excluding solutal buoyancy, respectively. Figure 11 (b) is a contour plot of the density in the buoyancy term of equation (1). Here, there is no contribution from solute, so the density varies linearly with temperature throughout the adiabatic zone to the interface. Figure 12 is a trace of density values along the centerline extracted from figures 6 (b) and 11 (b). Note the profound influence of solute on the density near the interface, when compared to the thermal convection only case. It is these density gradients which are the cause of the convective patterns observed in each case. Figure 13 (a) is a plot of concentration contours for the thermal

convection only case. The important detail to note is that even though $|U_{max}|$ is about the same for the cases including and excluding solutal convection, the maximum velocity within the solutal boundary layer is 3.61 times greater in the thermal convection only case; the higher level of convection has resulted in the concentration contours being slightly distorted. The contours now take on a very gentle "reverse-s" shape. Figure 13 (b) is a plot of isotherms for this case. Note that the minimum temperature (510 K) is lower than that found from the thermo-solutal case (512 K). This is expected and is due to the greater amount of solute transport by convection at the interface (recall that the melting temperature at the interface is dependent on the value of concentration). The isotherms near the interface are still flat. Figure 14 is a plot of concentration traces across the interface for the thermo-solutal convection case and the thermal convection only case. A diffusion-only case ($\theta = \pm 90^\circ$) is included to provide a basis for comparisons. Note the following dramatic difference between the concentration traces predicted by the two simulations. First, the locations of the maximum and minimum values of concentration have been transposed, such that the segregation is in the opposite sense. Second, the higher levels of convection near the interface have resulted in a higher maximum concentration (14.51 vs. 13.87 at.%) and a lower minimum (13.02 vs. 13.72 at.%). The value of radial solute segregation, ξ, is an order of magnitude higher, at 11.5%; and is considered large enough to represent a departure from diffusion dominated growth.

5.2 "g-jitter" Analysis

Transient simulations (including both thermal and solutal buoyancy) were performed to examine the system response to the application of a single **g** impulse. The **g** impulse vector was at an orientation of $\theta = 0^\circ$, with a magnitude of 100 μg and a duration of 1 second. This corresponds with standard orbital maneuvering. In addition, a steady **g** vector, at an orientation $\theta = 0^\circ$ and a magnitude of 1 μg, was applied for the entire duration of the simulation. This corresponds to the quasisteady **g** effect of tidal and aerodynamic drag forces as considered in section 5.1. The initial condition used for the solution was the steady state solution obtained for the corresponding case in section 5.1. The **g** impulse was applied from a simulation time of t = 0.0 to t = 1.0 second.

Figure 15 is a plot of velocity vectors at four selected times throughout the simulation. Figure 15 (a) is at a simulation time of 0.5 seconds, i.e. half way through the gravity pulse. The level of convection has increased significantly over the steady state result. The value of maximum velocity is 4.080 $\times 10^{-4}$ cm/s, which is *higher than the growth velocity*. The location of this maximum velocity has shifted to (x = 4.861 cm, y = 0.2333 cm). This is further from the centerline and closer to the interface than for the steady state case. Indeed, the entire convective motion is much stronger, as can be gleaned by perusing the plot. This trend continues for the plot shown in figure 15 (b). This figure is the velocity field at a time of t = 1.0 second, i.e. just as the pulse terminates. This is the time at which maximum velocities are found. The value of maximum velocity is 6.309 $\times 10^{-4}$ cm/s, which is 1.87 times the growth velocity. The location at which the maximum velocity acts is (x = 4.945 cm, y = 0.2333 cm). Figure 15 (c) shows the velocity vectors after 25.2 seconds. At this time, the strength of convection has decreased appreciably - the maximum value is 6.996 $\times 10^{-5}$ cm/s at (x = 5.237 cm, y = 0.1667 cm). The convective motions are similar to the steady state case although the magnitudes are higher. The final plot, figure 15 (d) is for a time of 126 seconds. At this time, the convective motion has almost been restored to steady state. The maximum velocity is 4.426 $\times 10^{-5}$ cm/s at (x = 5.132 cm, y = 0.1667 cm). This value is only 0.1% higher than that which occurs at steady state and is at the same location.

Figure 16 is a plot of radial solute segregation at the interface (as defined by equation 15) against time. The maximum value of segregation does not correspond to the time at which convection is a maximum; rather the maximum rate of increase in segregation occurs when convection levels are at their highest. The increased convection levels in the flow field from 0 to 126 seconds lead to increasing levels of radial solute segregation. The maximum segregation is found to be 1.31% , at a simulation time of t =126 seconds, when the level of convection is restored (almost) to the steady state value. After this time the level of segregation slowly decreases as the solute field slowly drifts toward its steady state configuration. Even though ξ has increased by about 30% due to the impulse, this level of segregation is still insignificant and would be within the scatter and uncertainty of a physical measurement. Post-flight measurements on a Bi- 0.1 at%Sn ingot solidified in space with similar g and g-jitter conditions have shown composition to increase from

about 0.01 at.% to 0.1 at.% along the centerline as a result of the g-jitter impulse [17]. Such a dramatic composition increase has not been predicted by the present work. Since the simulations performed were subject to steady state assumptions (refer to section 3), the authors suspect that all the important transport phenomena have not been modelled adequately. To do this a more detailed model is required which includes the presence of a solid phase and a moving solid/liquid interface. Such a model is unencumbered by steady state assumptions and should furnish results with better agreement with the experimental data.

Figure 17 is a plot of solute concentration traces across the interface at the simulation times considered above. The t = 0.5 and t = 1.0 second traces are almost indistinguishable from the steady state traces. Even though the convection is much higher at these times, the convective fields have not established themselves for a long enough period of time to have an impact of the solutal field. The t = 25.2 and t = 126 second traces show deviation from the steady state. Time has allowed the increased convection to alter the solute field. Also worthy of note is the asymmetry of the traces at the later times. The departure from the steady state case is less in the y = -0.3 to 0 cm section of the interface when compared to the y = 0 to 0.3 cm section of the interface. This could possibly indicate that the convective cell driven by thermal gradients is slightly dominant over the cell driven by solutal gradients at increased levels of convective strength.

6. CONCLUSIONS

The aim of these simulations was to quantify the effect of thermo-solutal convection on the MEPHISTO-4 space experiments. The results show that for all orientations of the steady state gravity vector of magnitude 1 μg the directional solidification process remains diffusion controlled. The maximum convective velocity was found to be 4.424×10^{-5} cm/s for the horizontal Bridgman growth configuration ($\theta = 0^{\circ}$). This value is an order of magnitude lower than the growth velocity of 3.38×10^{-4} cm/s. The maximum value of radial solute segregation (as defined by equation 15) was found to be $\xi = 1.046\%$. The radial segregation was such that the concentration at the interface decreased in the direction of applied gravity. A secondary

objective of this work was to compare results obtained including solutal convection with those that consider thermal convection only. This work indicated that the addition of solutal convection had a profound effect of the convective flow patterns and the resulting levels of radial segregation at the interface. Simulations that ignored solutal convection were found to overpredict the level of radial segregation by an order of magnitude and to reverse the concentration profile at the interface, with concentration at the interface increasing in the direction of applied gravity.

The final component of the present study was to examine the effect of g-jitter. For a 100 μg gravity pulse of duration 1 second and acting normal to the direction of growth, the process remains diffusion controlled. The level of radial solute segregation increased to a peak value of ξ = 1.31%. The maximum level of convection was found to be 6.309 $\times$ 10^{-4} cm/s at a simulation time of t = 1 sec (i.e. at the time when the pulse terminated). After 126 seconds, the level of convection had returned to a value of 4.426 $\times$ 10^{-5} cm/s which is within 0.1% of the initial steady state value. This was the time at which maximum radial solute segregation was observed. After this time, the level of radial segregation slowly decreased, to a value of 1.11% at 1140 seconds (the simulation finish time).

7. POSTSCRIPT

There is a subtle and significant nuance to the use of β_C and C in equation (1). As defined, β_C is equal to $d\rho/dC$ divided by ρ_0. In practice however, β_C is determined as $(\rho_2-\rho_1)/\rho_1(C_2-C_1)$ where ρ_1 and ρ_2 are the densities of the pure solvent and solute respectively, and C_1 and C_2 are the compositions of the pure solvent and solute respectively. Note that C_1 and C_2 are always equal to 0 and 100% respectively. In using $(\rho_2-\rho_1)/\rho_1(C_2-C_1)$, a linear relation is assumed between density and composition in the units of C. This assumption is valid, in general, when the units of C are in volume percent (or fraction) [18]. We used atomic fraction which exaggerated the influence of solute in the density of the liquid in (1). However, since the flow is nearly negligible, and growth was determined to be dominated by diffusion, this error is not considered significant to the major conclusions of this work.

8. ACKNOWLEDGEMENTS

We would like to thank and acknowledge the support of Tom Glasgow, the Microgravity Science Division, and the Microgravity Science and Applications Division for their support of this work. Thanks are also due the Principal Investigator of the MEPHISTO-4 Shuttle Flight experiment, Prof. Reza Abbaschian, University of Florida at Gainesville; and Co-Investigator Prof. Graham de Vahl Davis and his team at the University of New South Wales, Australia.

REFERENCES

[1] R. Abbaschian, A.B. Gokhale, J.J. Favier and S.R. Coriell, "In-Situ Monitoring of Crystal Growth Using MEPHISTO," *NASA Science Requirements Document (SRD),* October 1992.

[2] R. Abbaschian, A.B. Gokhale, and D.B. Allen, "A study of Directional Solidification of Faceted Bi-Sn Alloys in Microgravity," *Solidification Science and Processing*, Edited by I. Ohnaka and D.M. Stefanescu, 1996, p.73.

[3] M. Yao and H.C. de Groh III, "Three-Dimensional Finite Element Method Simulation of Bridgman Crystal Growth and Comparison With Experiments," *Numerical Heat Transfer, Part A,* Vol. 24, pp. 393-412, 1993.

[4] H.C. de Groh III and E.S. Nelson, "On Residual Acceleration During Space Experiments," in *Heat Transfer in Microgravity Systems*, S.S Sadhal and A. Gopinath, eds., ASME HTD-Vol. 290, pp. 23-33, 1994.

[5] J.I.D. Alexander, "Response of Crystal Growth Experiments to Time-Dependent Residual Accelerations," in *Materials and Fluids Under Low Gravity,* edited by L. Ratke, H. Walter and B. Feuerbacher, Springer, 1995.

[6] J.I.D. Alexander, J. Ouazzani and F. Rosenberger, "Analysis of the Low Gravity Tolerance of Bridgman-Stockbarger Crystal Growth," *Journal of Crystal Growth,* Vol. 97, pp. 285-302, 1989.

[7] M. Yao, R. Raman and H.C. de Groh III, "Numerical Modeling of Heat and Mass Transport During Space Crystal Growth with MEPHISTO," *NASA TM 107015,* 1995.

[8] P. Chen, G. de Vahl Davis, J. Kaenton, E. Leonardi, S.S. Leong, V. Timchenko, H.C. de Groh III, and R. Abbaschian, "Rehomogenization: Diffusion and Convection in Microgravity" AIAA 98-0740, Accepted for publication at the *36th Aerospace Sciences Meeting & Exhibit,* Reno, Nevada, AIAA, January 1998.

[9] M. Yao, H.C. de Groh III and R. Abbaschian, "Numerical Modeling of Solidification in Space with MEPHISTO-4 (Part 1)," Presented at the *35th Aerospace Sciences Meeting & Exhibit,* Reno, Nevada. AIAA 97-0449, January 1997.

[10] W. Kurz, and D.J. Fisher, *Fundamentals of Solidification*, Trans Tech Publications, 1989.

[11] M.C. Flemings, *Solidification Processing,* McGraw-Hill, 1974.

[12] M. Engleman, *FIDAP 7.0 Theory Manual*, Fluid Dynamics International, Inc., Evanston, IL, 1993.

[13] R. Barrett, M. Berry, T.F. Chan, J. Demmel, J. Donato, J. Dongarra, V. Eijkhout, R. Pozo, C. Romine and H. Van der Vorst, *Templates for the Solution of Linear Systems: Building Blocks for Iterative Methods,* SIAM, Philadelphia, PA, 1994

[14] J.E. Simpson and S.V. Garimella, "An Investigation of the Solutal, Thermal, and Flow Fields in Unidirectional Alloy Solidification," *International Journal of Heat and Mass Transfer*, accepted for publication, 1997.

[15] G. de Vahl Davis, "Natural Convection of Air in a Square Cavity: a Bench Mark Solution," *International Journal of Numerical Methods in Fluids* Vol. 3, pp. 249-264, 1983.

[16] F. Stella, G. Guj and E. Leonardi, "The Rayleigh-Bénard problem in intermediate bounded domains," *Journal of Fluid Mechanics*, vol. 254, pp. 375-400, 1993.

[17] R. Abbaschian, unpublished work, 1996.

[18] L.H. Van Vlack, A Textbook of Materials Technology, Addisom-Wesley, pp. 90, 1973.

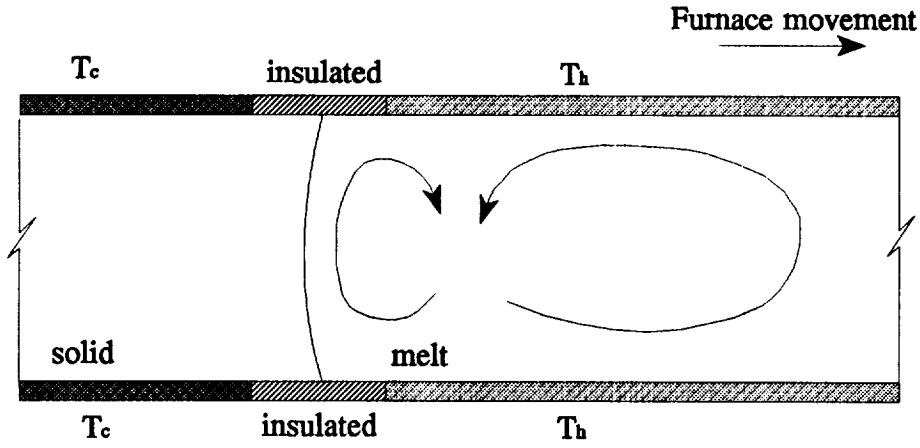

Figure 1. Schematic of Bridgman crystal growth process.

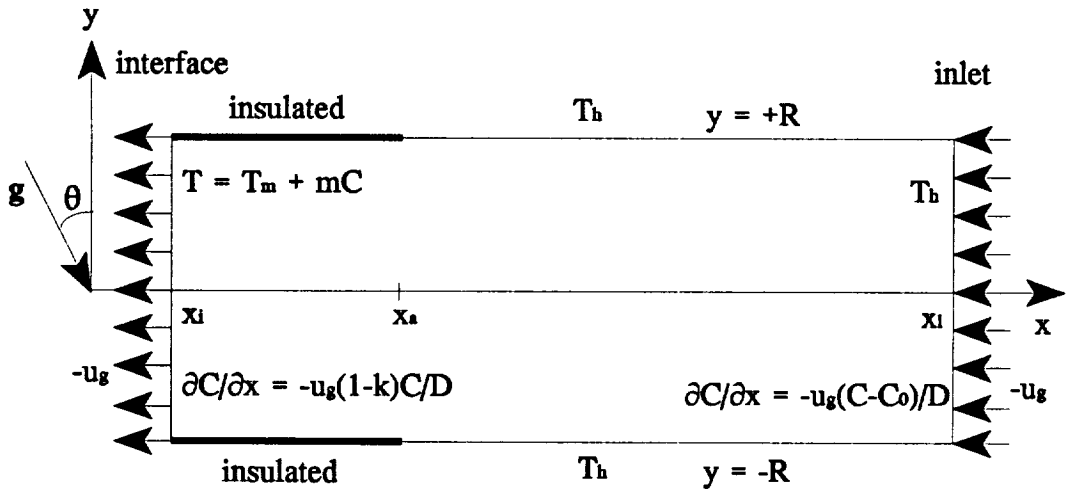

Figure 2. Computational domain for pseudo-steady state model, including pertinent boundary conditions. Angle θ is defined as the angle from the y-axis to the gravity vector, counter-clockwise positive. This results in the gravity force components $g_x = g \sin \theta$, $g_y = -g \cos \theta$.

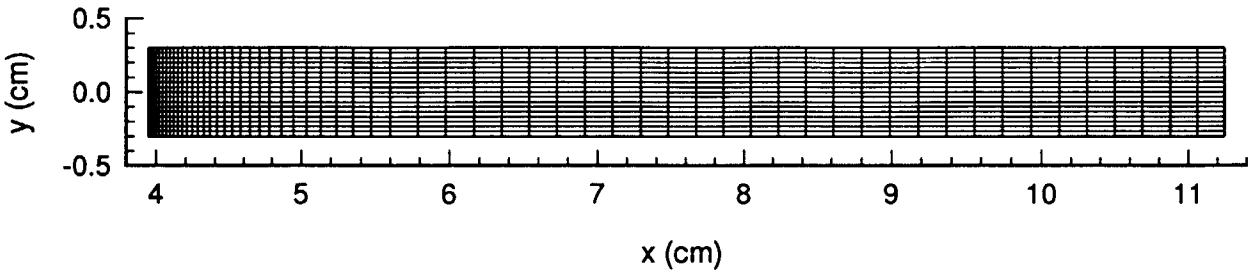

Figure 3. The finite element mesh employed for the analysis. Note the grading of the mesh as it approaches the interface. This is to adequately resolve solutal concentration gradients near the interface. The aspect ratio (length:height) of the cavity is 12.17:1.

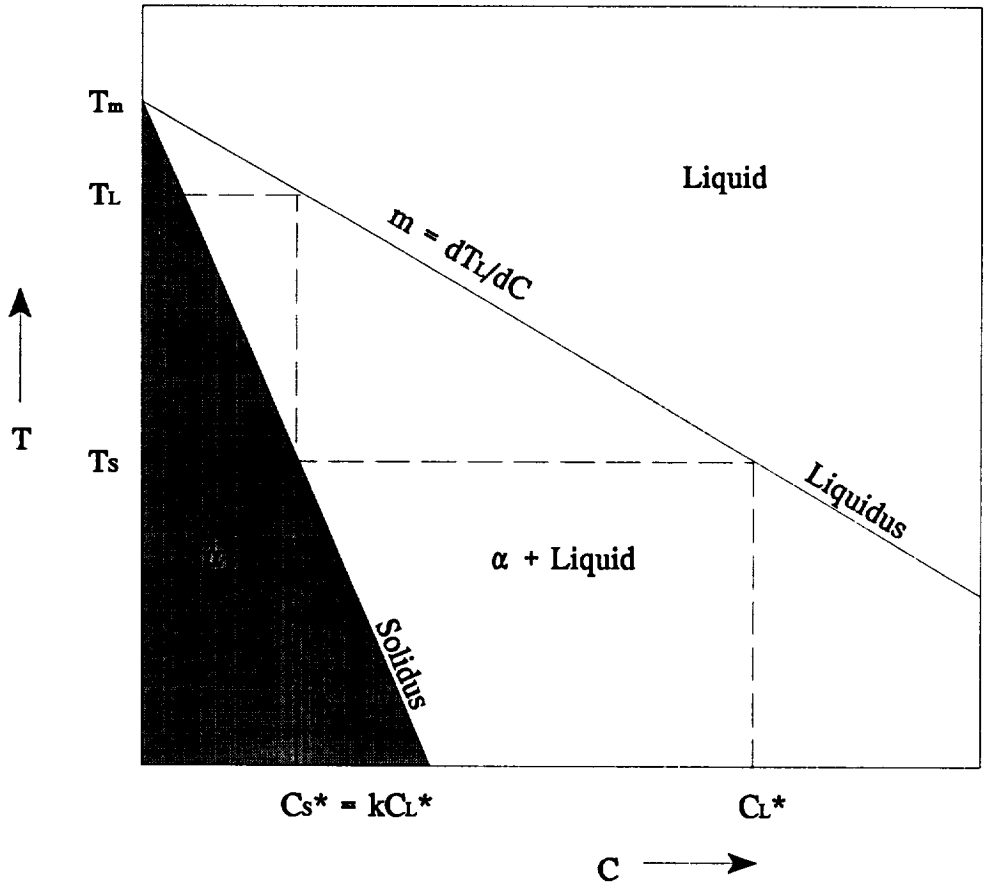

Figure 4. Bi rich portion of the linearized BiSn binary alloy phase diagram. The change in melting temperature of the alloy with increasing tin composition is given by the slope of the liquidus line, m. The composition of the liquid at the interface (C_L^*) and the composition of the solid at the interface (C_S^*) is related by the segregation coefficient, k.

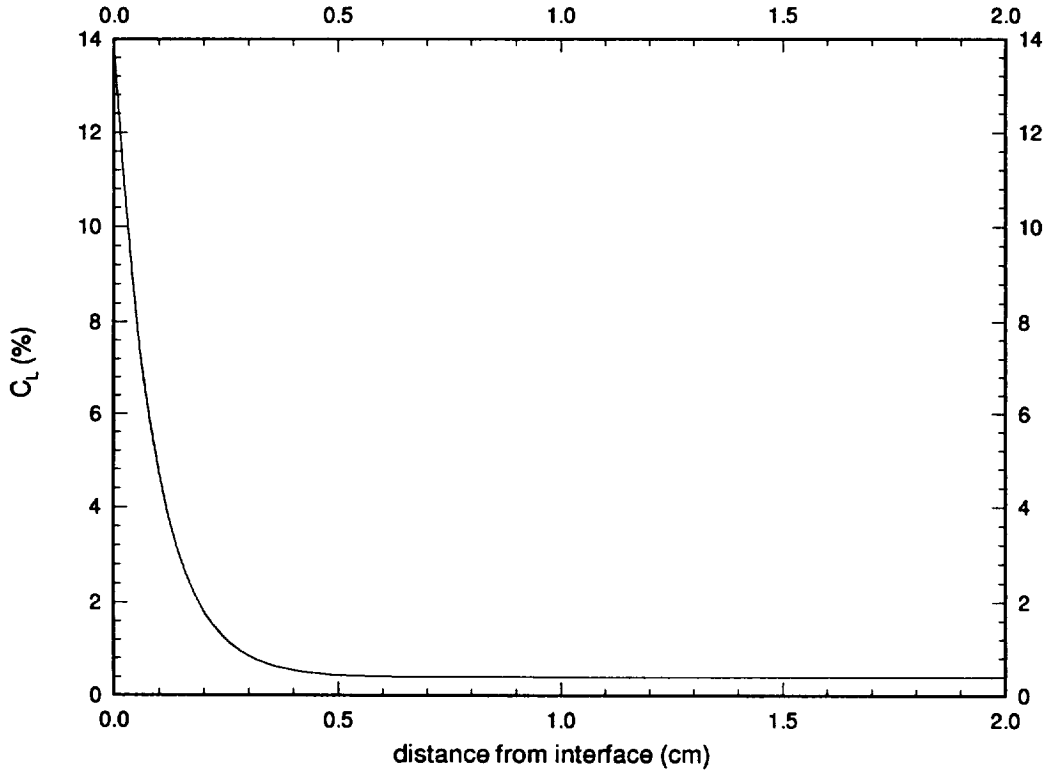

Figure 5. Steady state solute concentration profile in the liquid domain from diffusion based analytical result.

θ = 0, 1 μg

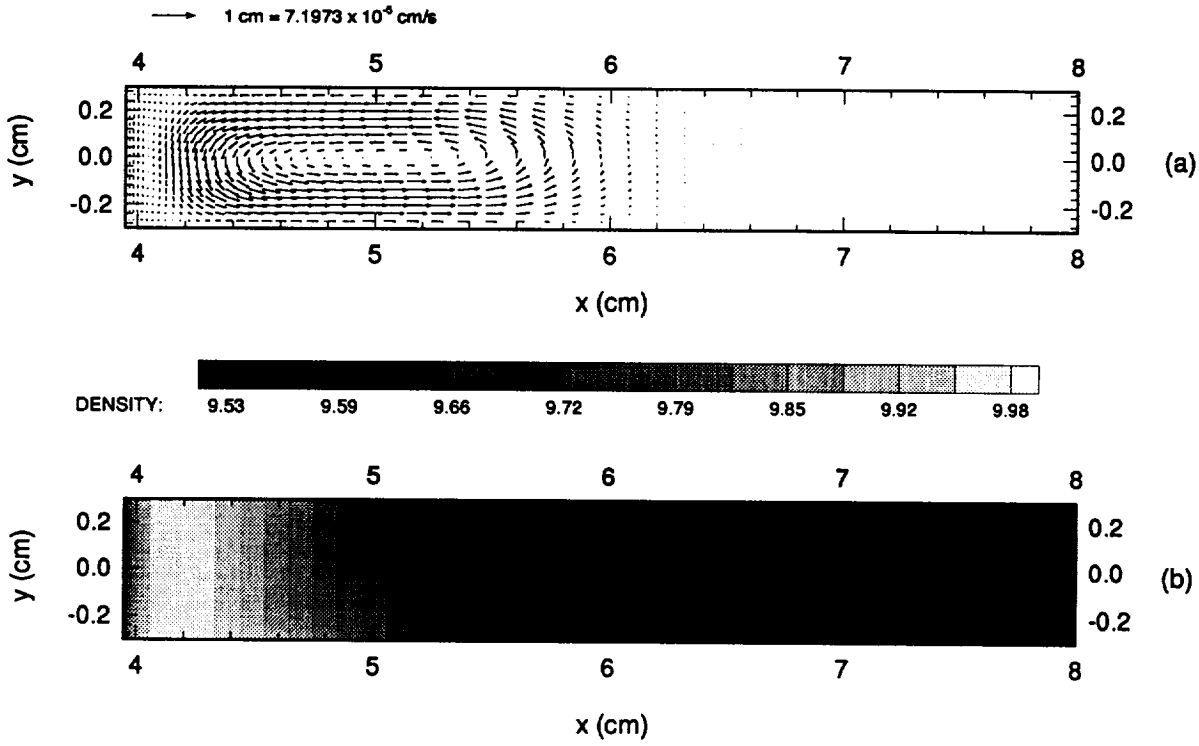

Figure 6. (a) Velocity vectors for $\theta = 0^{\circ}$ simulation, including the effects of buoyancy due to temperature and solute. The growth velocity, u_g, has been eliminated from the x-component of velocity for this and subsequent velocity plots so the true nature of the convective flow can be revealed. Two convective cells can be discerned, one small, clockwise rotating cell next to the interface and a large counter-clockwise rotating cell. (b) A contour plot of the value of density used in the buoyancy term of equation (1). This indicates the gradients which motivate the convective flow seen in (a).

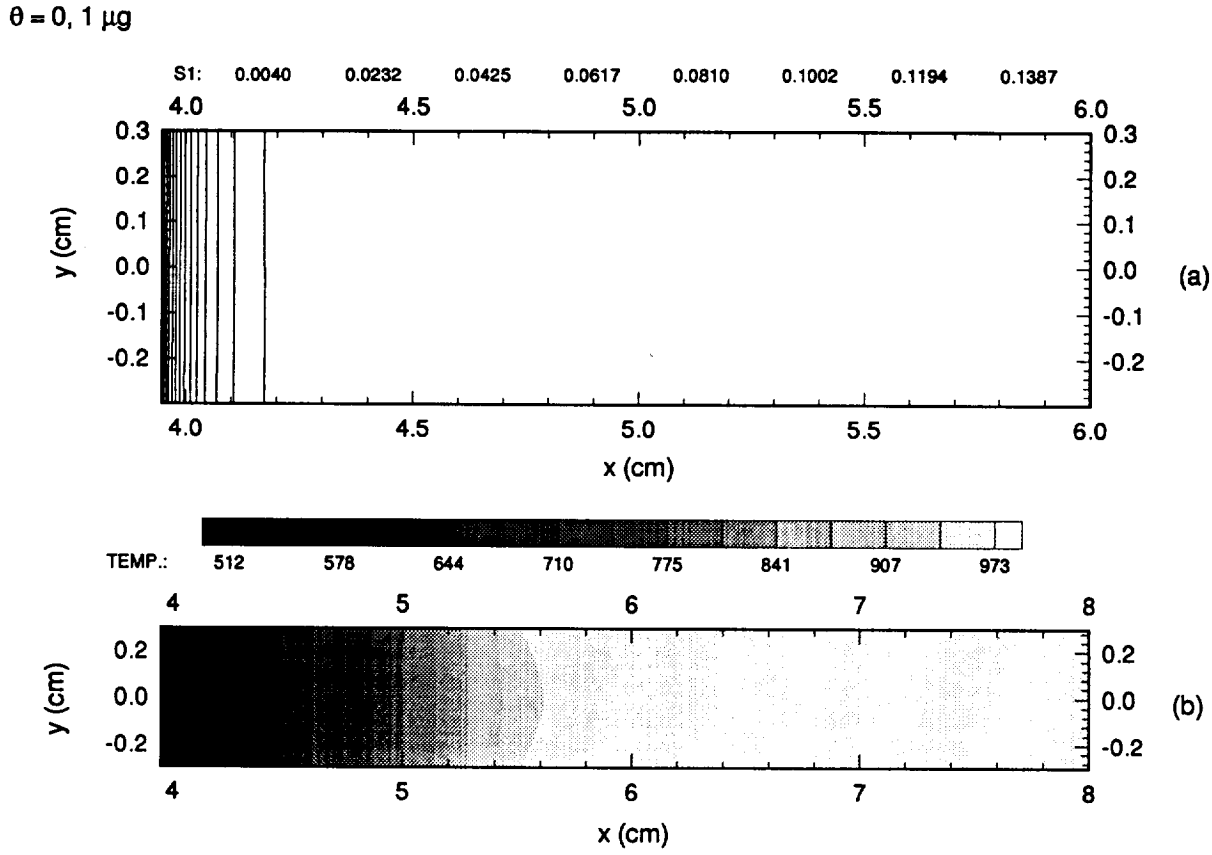

Figure 7. (a) Contour plot of solute concentration. Note the high gradients near the interface and that the lines have barely deflected from the vertical. (b) Contour plot of temperature throughout the simulation domain. Note the suppression of interface temperature from the zero concentration value of T_m = 544.3 K.

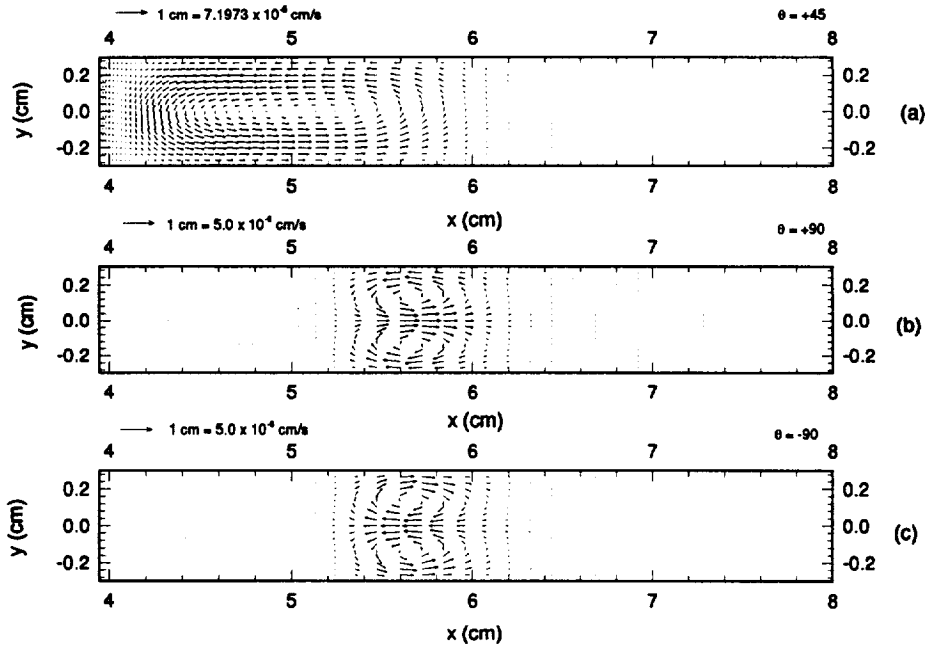

Figure 8. Vector plots for (a) $\theta = +45^{\circ}$, (b) $\theta = +90^{\circ}$ and (c) $\theta = -90^{\circ}$ cases. Note the different scales for the velocity vectors.

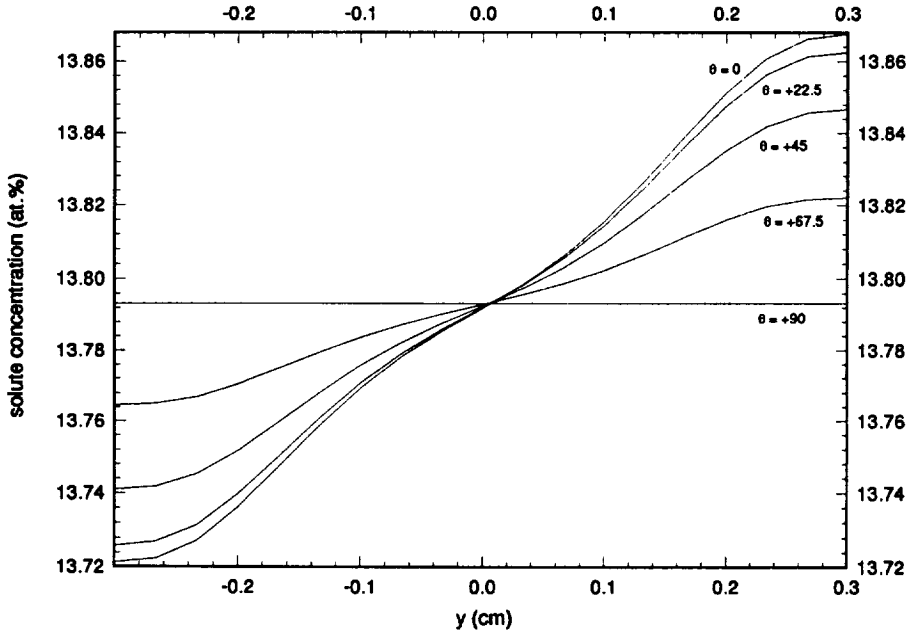

Figure 9. Solute concentration plot across the interface, in the liquid, for each orientation. The "bottom" of the interface is to the left (y = -0.3 cm), the "top" is to the right (y = +0.3 cm).

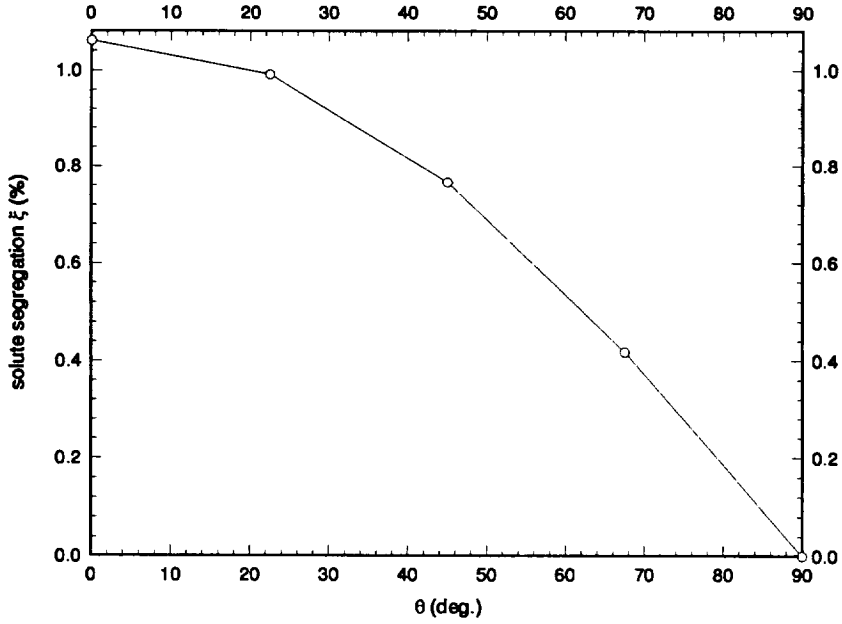

Figure 10. Solute segregation vs gravity vector angle. Segregation is at a maximum for horizontal Bridgman growth (θ = 0°).

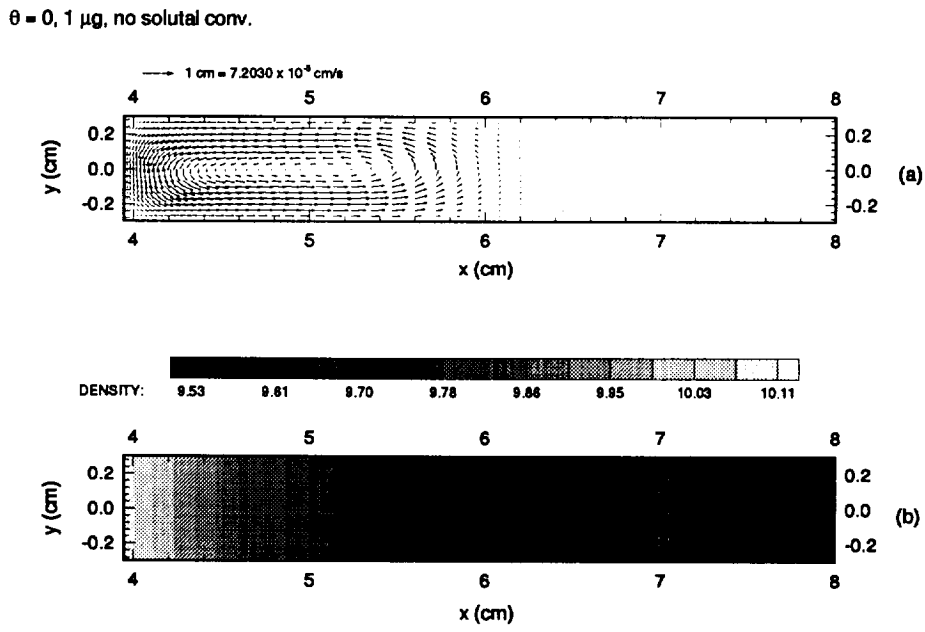

Figure 11. (a) Velocity vectors for θ = 0° simulation, ignoring solutal convection. Only one convective cell exists. (b) A contour plot of the value of density used in the buoyancy term of equation (1). This indicates the gradients which motivate the convective flow seen in (a).

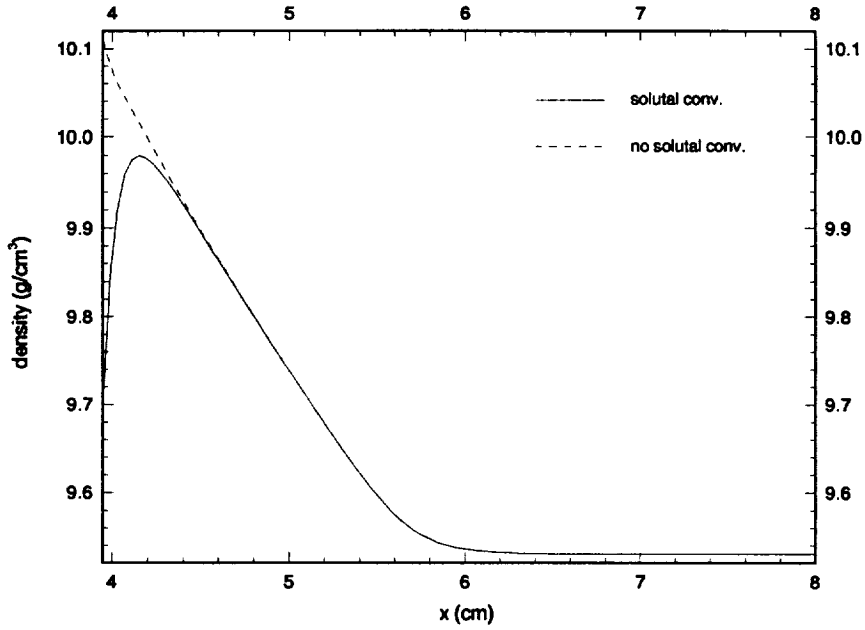

Figure 12. Trace of density along the centerline taken from figures 6 (b) and 11 (b). The presence of volumetric expansion due to solute concentration can clearly be seen.

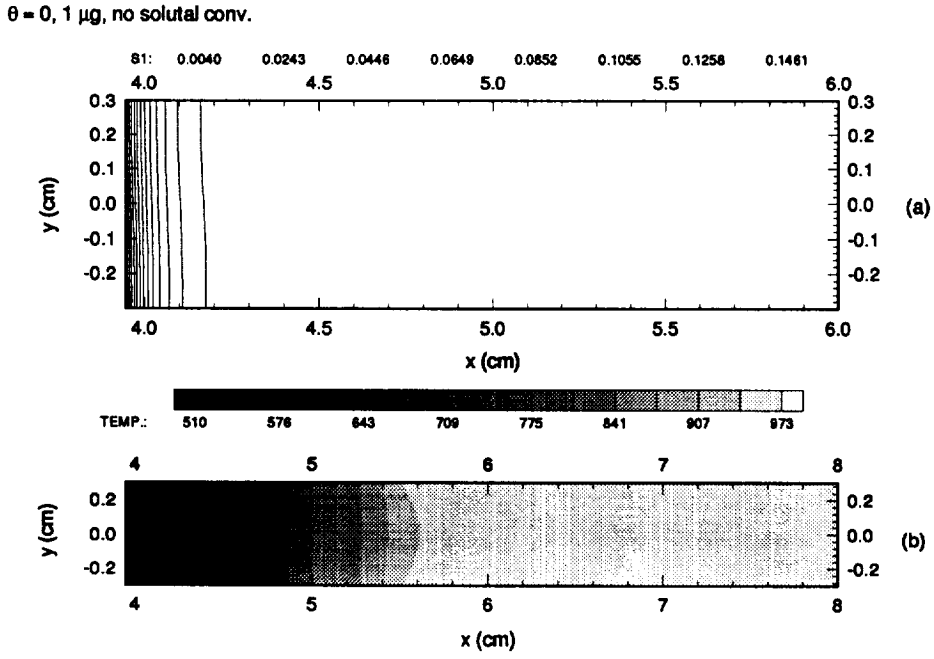

Figure 13. (a) Contour plot of solutal concentration. The lines exhibit some deflection from the vertical. (b) Contour plot of temperature throughout the simulation domain. Note the minimum interface temperature is lower (510 K) than that for the case with solutal convection (512 K).

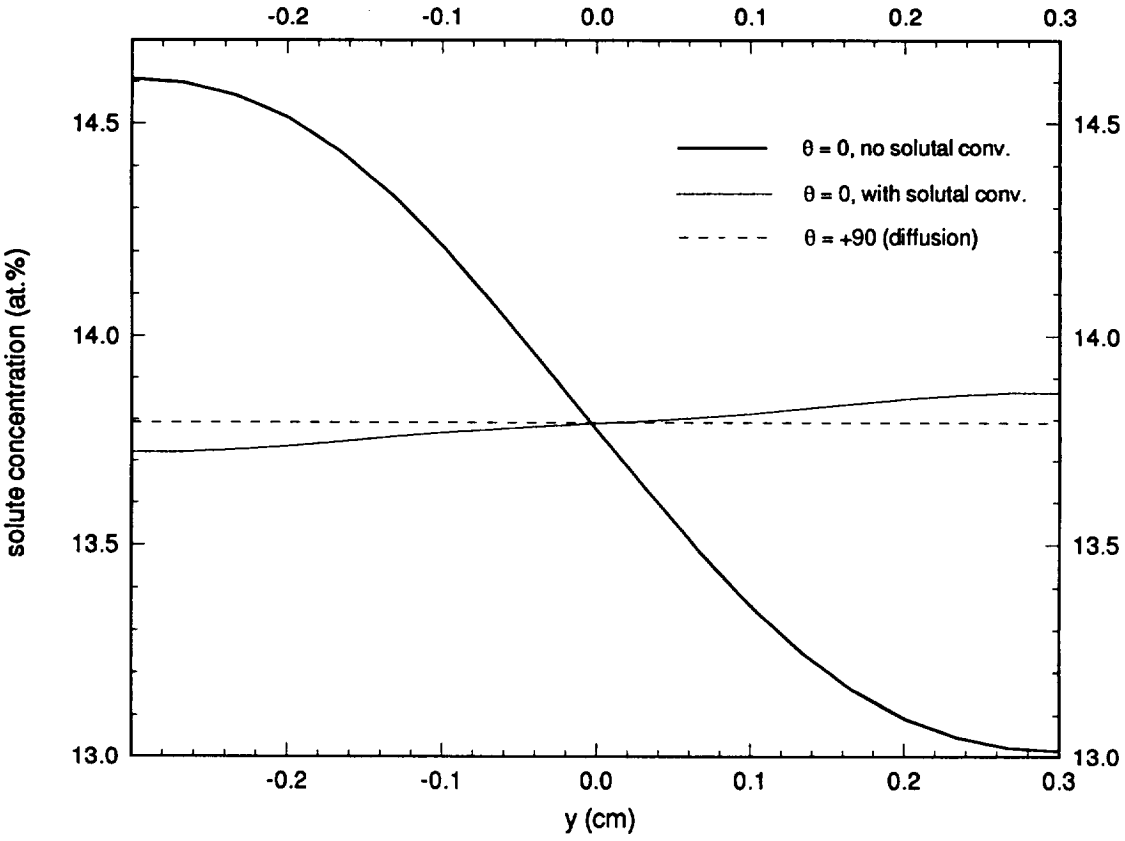

Figure 14. Comparison of the calculated solutal distributions at the interface. The results are significantly different for the two cases.

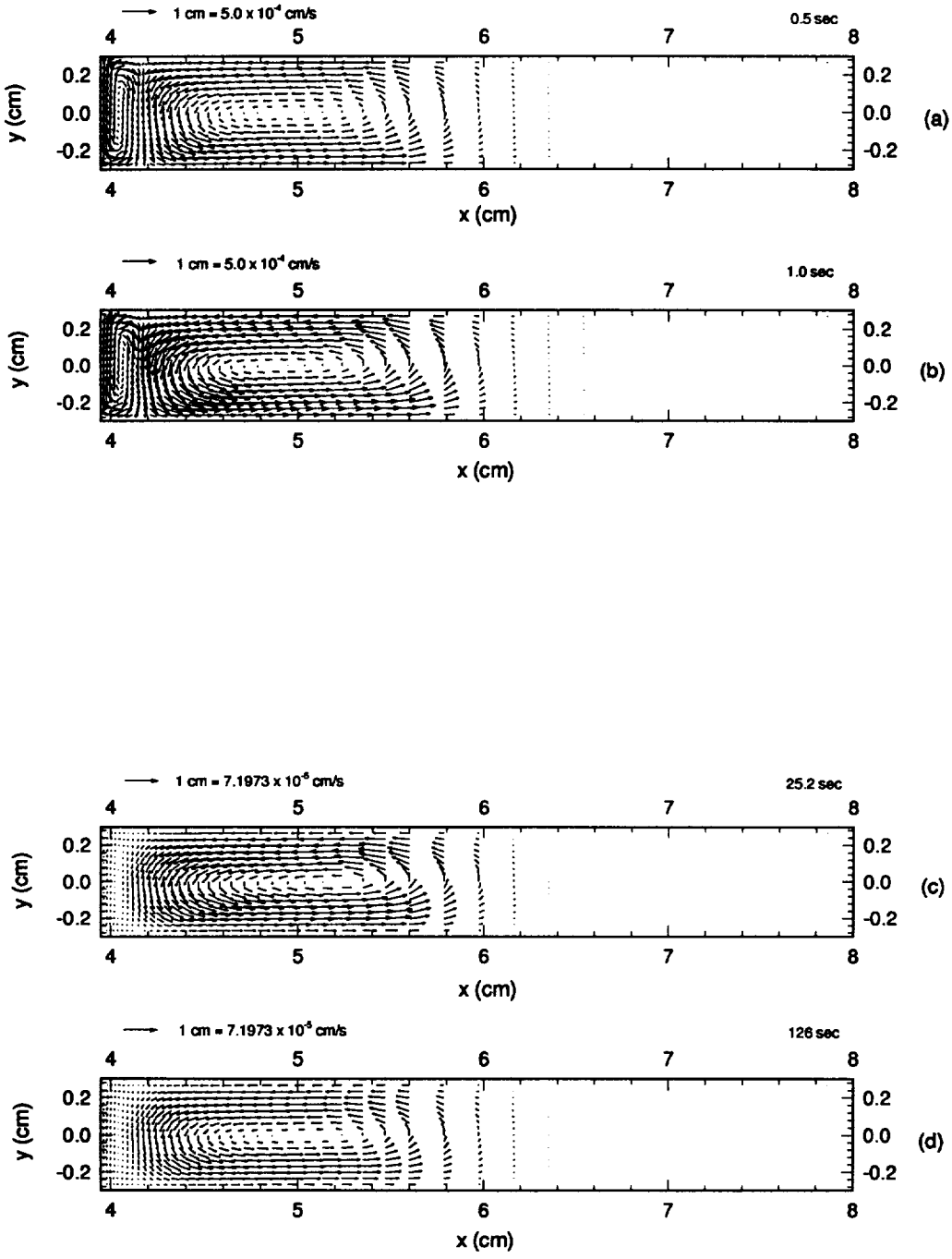

Figure 15. Velocity vectors for a simulation time of (a) t = 0.5 sec, (b) t = 1.0 sec, (c) t = 25.2 sec and (d) t = 126 sec. Note the different scales used for the vector magnitudes.

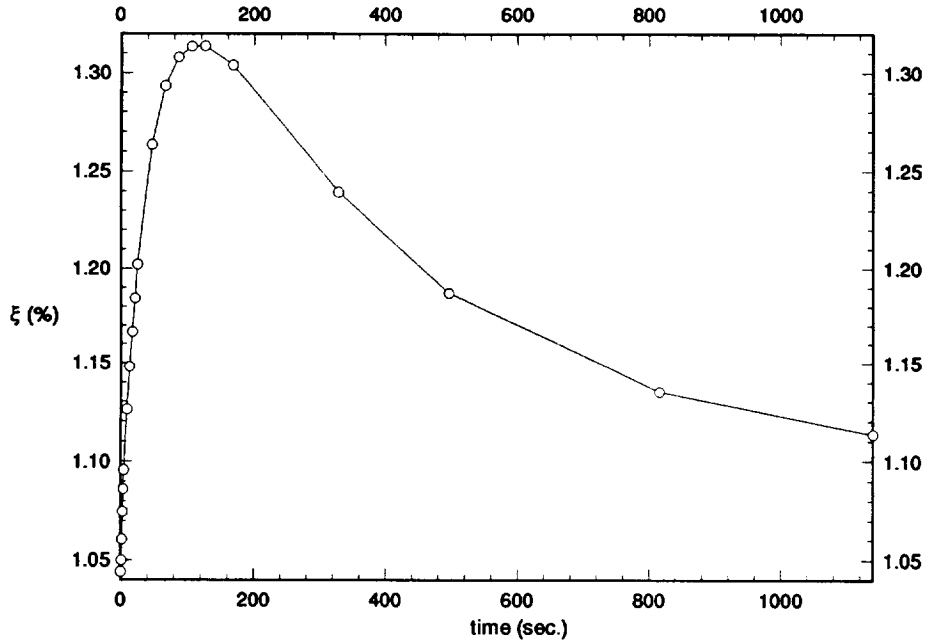

Figure 16. Plot of radial segregation, ξ, across the interface agianst simulation time, after a g-jitter impulse of 100 μg for 1 second starting at t = 0.

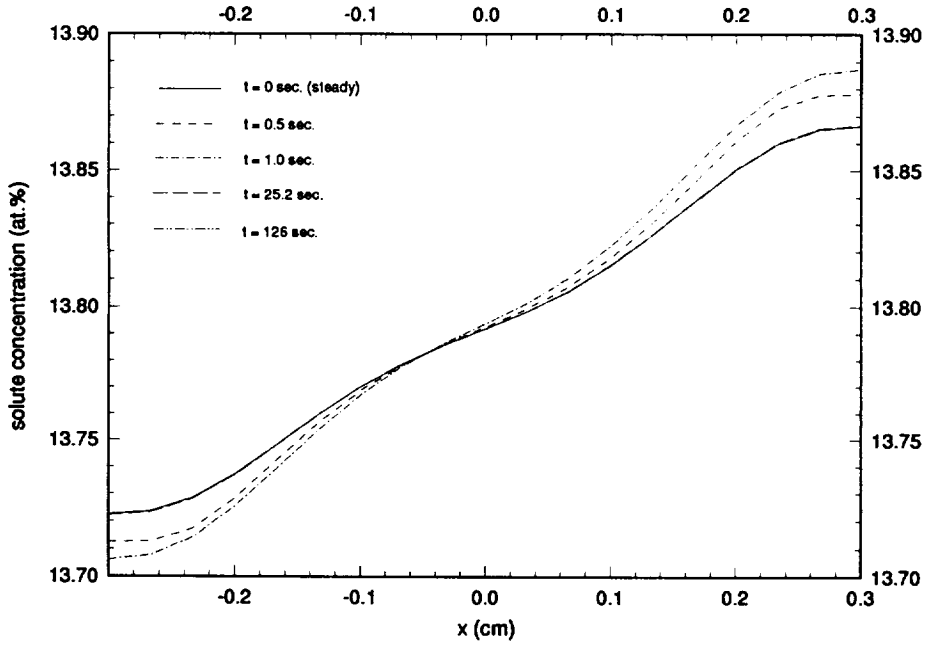

Figure 17. Solute concentration traces at the interface at various times. Note that the solid line for the steady state solution effectively blanks out the lines for t = 0.5 and t = 1.0 second.

APPENDIX A

(following 5 pages)

ADDITIONAL PLOTS

AND

TABLE OF PERTINENT THERMOPHYSICAL PROPERTIES & CONSTANTS

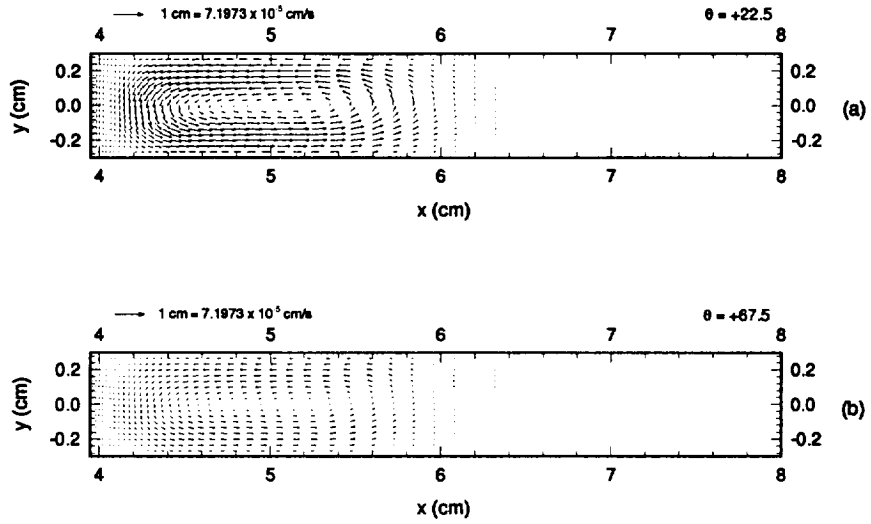

Figure A1. Velocity vectors for simulations with solutal convection for (a) $\theta = +22.5^{\circ}$ and (b) $\theta = +67.5^{\circ}$ cases. The character of convective motion is similar in both cases, but note the difference in magnitude of velocities. Contour plots of density, temperature and solute concentration are not discernably different to those shown in figure 6b and 7, and so are not provided.

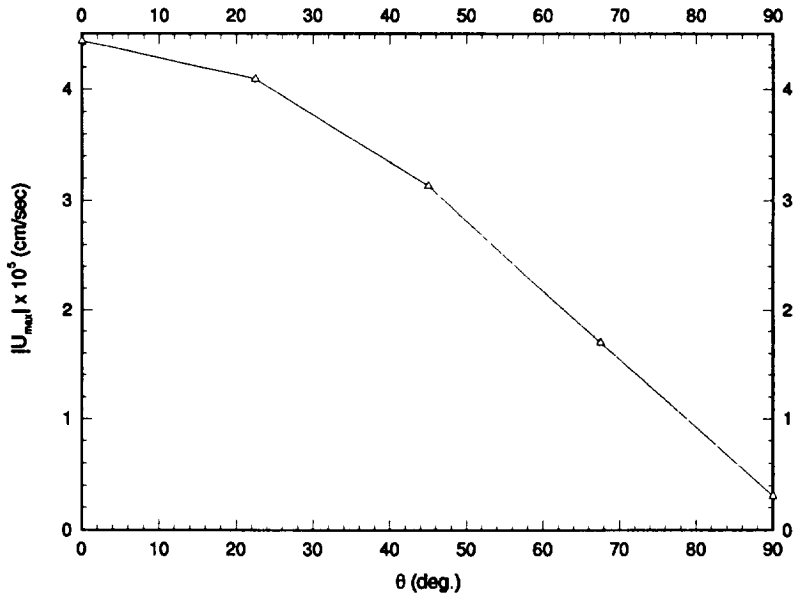

Figure A2. Plot of the maximum magnitude of velocity vs gravity vector angle. Maximum convective motion occurs during horizontal ($\theta = 0^{\circ}$) Bridgman growth.

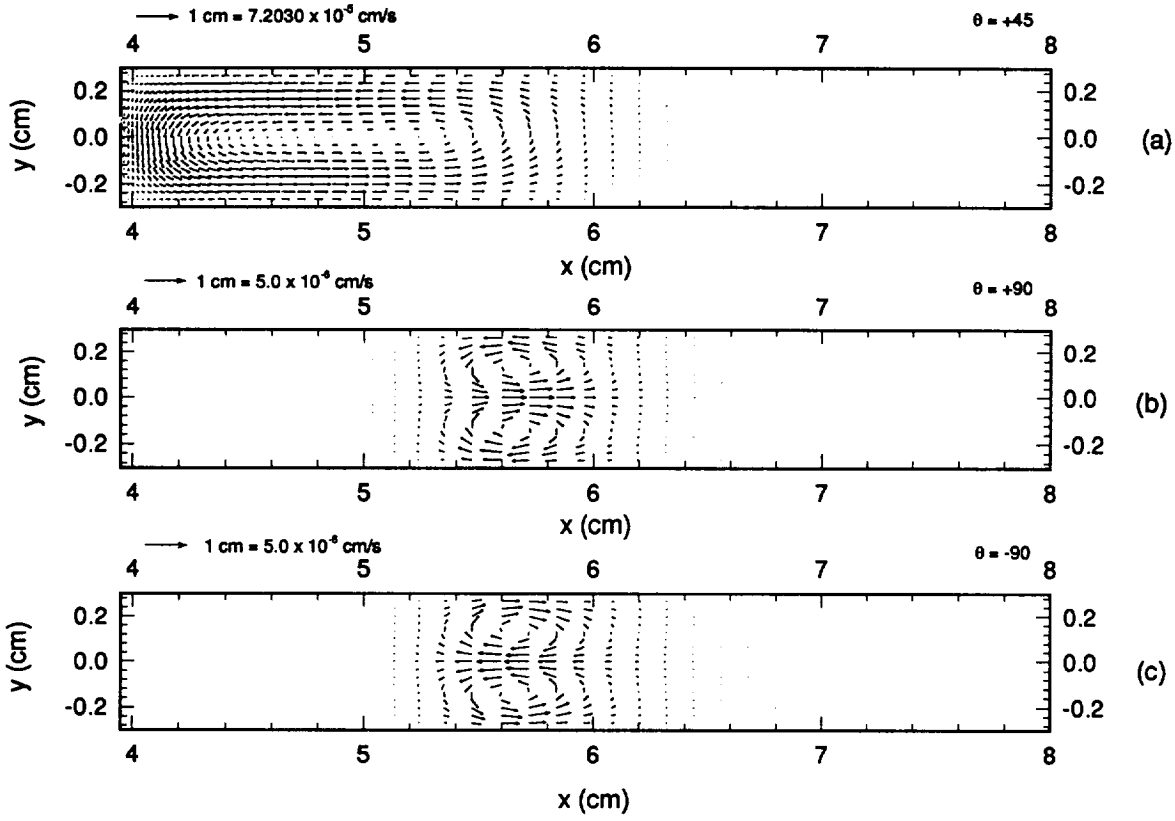

Figure A3. Velocity vectors for simulations **without** solutal convection for (a) θ = +45°, (b) θ = +90° and (c) θ = -90° cases. Figures A3 (b) and (c) are very similar to figures 8a and b, and the phenomena at the interface are absent from the effects of convection.

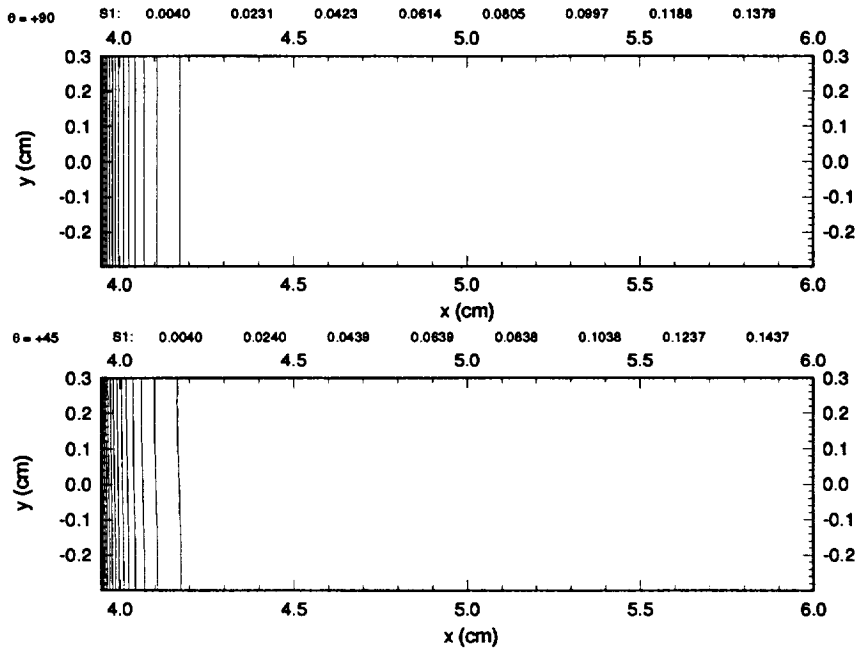

Figure A4. Concentration contours for simulations **without** solutal convection for (a) θ = +90° and (b) θ = +45° orientations. Contours for the -90° case are identical to the +90° case and so are not presented.

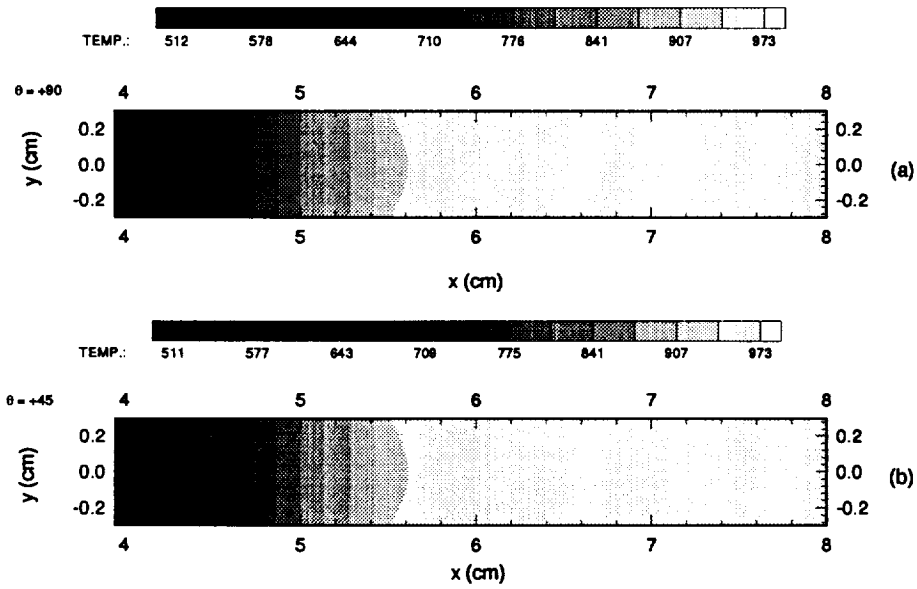

Figure A5. Temperature contours for simulations **without** solutal convection for (a) θ = +90° and (b) θ = +45° orientations. Again, contours for the -90° case are superfluous.

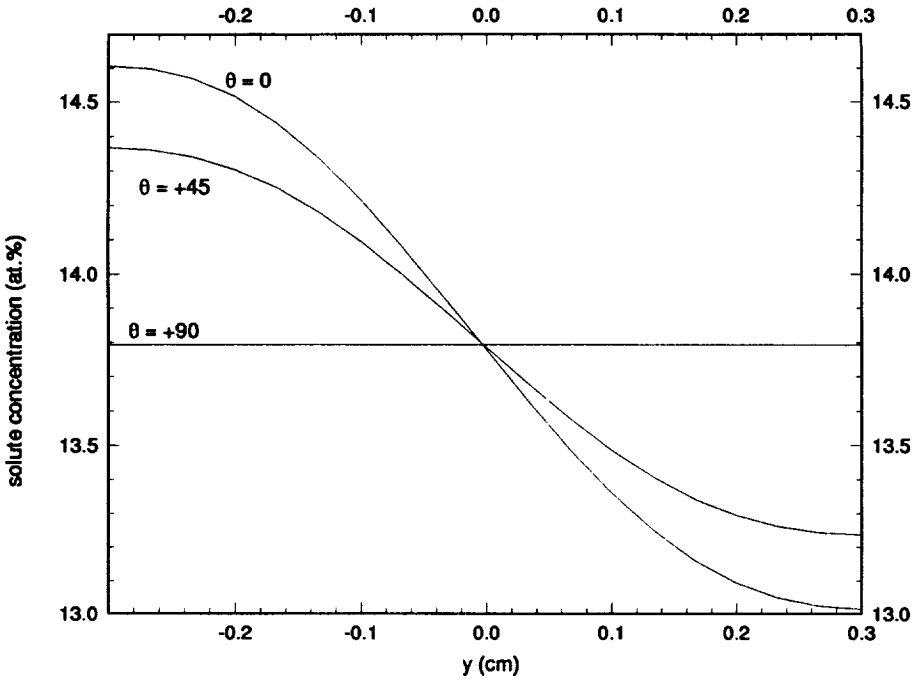

Figure A6. Solute concentration traces at the interface for simulations **without** solutal convection. Note the sinusoidal shape of the curves.

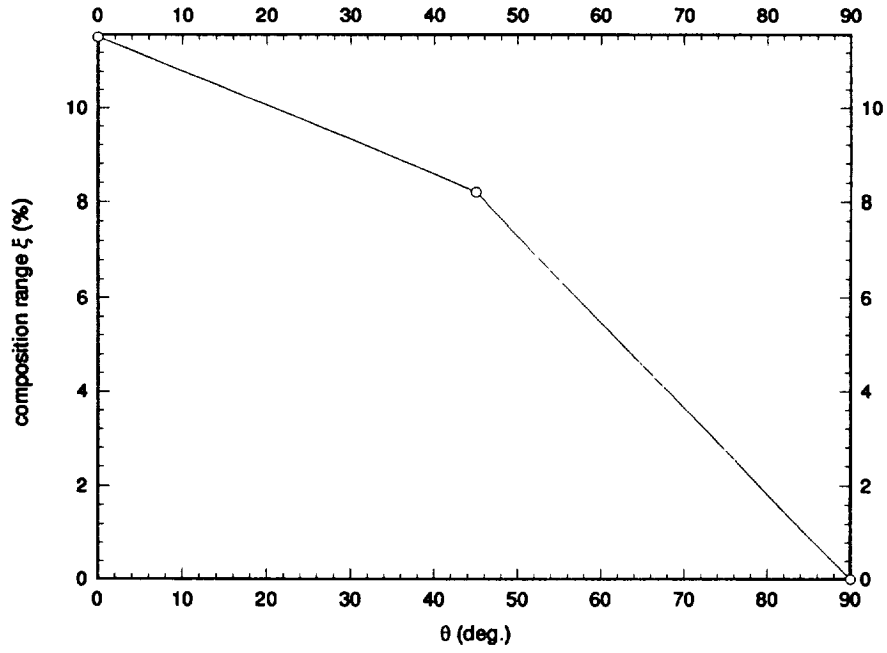

Figure A7. Solute segregation values for each simulation **without** solutal convection.

Table A1. Thermophysical properties and other pertinent physical values.

Quantity	Units	Value
Microgravity, μg	cm/s^2	980.6×10^{-6}
Hot furnace temperature, T_h	K	971.3
Melting tempearture of pure Bi, $T_m = T_0$	K	544.3
Furnace thermal gradient, dT/dx	K/cm	260
Slope of Liquidus line, m	K/(at. frac.)	-232.1
Initial solute concentration, C_0	at.%	0.4
Density of Bi at reference state, ρ_0	g/cm^3	10.07
Growth velocity, u_g	cm/s	$+3.38 \times 10^{-4}$
Thermal expansivity, β_T	K^{-1}	1.25×10^{-4}
Solutal expansivity, β_C	$(\text{at. frac.})^{-1}$	0.305
Distribution coefficient, k	at.%/at.%	0.029
First coefficient of viscosity of Bi, μ	cP	0.4458 exp[1.541 kcal-mol^{-1}/RT]
Diffusivity of Sn in liquid Bi, D	cm^2/s	5.2×10^{-4} exp[-3.2 kcal-mol^{-1}/RT]
Thermal conductivity, κ	W/cmK	
at 545 K		0.124
573 K		0.131
700 K		0.141
800 K		0.15
900 K		0.159
Specific heat at constant pressure, c_p	cal/gK	
at 545 K		0.0346
600 K		0.0336
700 K		0.0326
800 K		0.0321

REPORT DOCUMENTATION PAGE

Form Approved
OMB No. 0704-0188

1. AGENCY USE ONLY (*Leave blank*)	2. REPORT DATE	3. REPORT TYPE AND DATES COVERED
	February 1998	Technical Memorandum

4. TITLE AND SUBTITLE

Numerical Modeling of Solidification in Space With MEPHISTO-4 (Part 2)

5. FUNDING NUMBERS

WU-963-35-0F-00

6. AUTHOR(S)

James E. Simpson, Minwu Yao, Henry C. de Groh III, Suresh V. Garimella

7. PERFORMING ORGANIZATION NAME(S) AND ADDRESS(ES)

National Aeronautics and Space Administration
Lewis Research Center
Cleveland, Ohio 44135-3191

8. PERFORMING ORGANIZATION REPORT NUMBER

E-11081

9. SPONSORING/MONITORING AGENCY NAME(S) AND ADDRESS(ES)

National Aeronautics and Space Administration
Washington, DC 20546-0001

10. SPONSORING/MONITORING AGENCY REPORT NUMBER

NASA TM—1998-206630

11. SUPPLEMENTARY NOTES

James E. Simpson and Suresh V. Garimella, University of Wisconsin, P.O. Box 784, Milwaukee, Wisconsin 53201 (work funded under LSN000705); Minwu Yao, Ohio Aerospace Institute, 22800 Cedar Point Road, Brook Park, Ohio 44142; and Henry C. de Groh III, NASA Lewis Research Center, Cleveland, Ohio. Responsible person, Henry C. de Groh III, organization code 6712, (216) 433-5025.

12a. DISTRIBUTION/AVAILABILITY STATEMENT

Unclassified - Unlimited
Subject Category: 29 Distribution: Nonstandard

This publication is available from the NASA Center for AeroSpace Information, (301) 621-0390.

12b. DISTRIBUTION CODE

13. ABSTRACT ***(Maximum 200 words)***

A pre-flight analysis of the directional solidification of BiSn with MEPHISTO-4 is presented. Simplified Bridgman growth under microgravity conditions is simulated using a two dimensional finite element model. This numerical model is a single domain, pseudo-steady state model, and includes the effects of both thermal and solutal convection. The results show that for all orientations of the applied steady state gravity vector, of magnitude 1 μg, the directional solidification process remains diffusion controlled. The maximum convective velocity was found to be 4.424×10^{-5} cm/s for the horizontal Bridgman growth configuration. This value is an order of magnitude lower than the growth velocity. The maximum and minimum values of solute concentration in the liquid at the crystal-melt interface were 13.867 at.% and 13.722 at.%, respectively. This gives a radial segregation value of ξ = 1.046% at the interface. A secondary objective of this work was to compare the results obtained to those that consider thermal convection only (no solutal convection). It was found that the convective flow patterns in simulations which included solutal convection were significantly different from those which ignored solutal convection. The level of radial segregation predicted by the current simulations is an order of magnitude lower than that found in simulations which ignore solutal convection. The final aim was to investigate the effect of g-jitter on the crystal growth process. A simulation was performed to calculate the system response to a 1 second, 100 μg gravity impulse acting normal to the direction of growth. This pulse is consistent with that induced by Orbiter thruster firings. The results obtained indicate that such a gravity pulse causes an increase in the level of radial solute segregation at the interface from the steady state values. The maximum value of solute concentration in the liquid was found to be 13.888 at.%, the minimum value calculated was 13.706 at.%, yielding a radial segregation value of ξ = 1.31% at the interface. These values occurred 126 seconds after the pulse terminated. Thus it is anticipated that the process will remain diffusion controlled even when subjected to such g-jitter.

14. SUBJECT TERMS	15. NUMBER OF PAGES
Bismuth; Tin; Bi; Sn; Solute convection; Segregation; Bridgman; directional solidification	49
	16. PRICE CODE: A03

17. SECURITY CLASSIFICATION OF REPORT	18. SECURITY CLASSIFICATION OF THIS PAGE	19. SECURITY CLASSIFICATION OF ABSTRACT	20. LIMITATION OF ABSTRACT
Unclassified	Unclassified	Unclassified	